/inil

//

/ REF.

4063

591

FINAL TECHNICAL REPORT

Wave Generation by Contaminant Ions Near a Large Spacecraft

NASA/Lewis Research Center Grant NAG3-1373

Principal Investigator: N. Singh

Department of Electrical and Computer Engineering
The University of Alabama in Huntsville
Huntsville, Alabama 35899

Abstract

Measurements from the space shuttle flights have revealed that a large spacecraft in a low earth orbit is accompanied by an extensive gas cloud which is primarily made up of water. The charge exchange between the water molecule and the ionospheric O^+ ions produces a water ion beam traversing downstream of the spacecraft. In this report we present results from a study on the generation of plasma waves by the interaction of the water ion beams with the ionospheric plasma. Since velocity distribution function is key to the understanding of the wave generation process, we have performed a test particle simulation to determine the nature of H_2O^+ ions velocity distribution function. The simulations show that at the time scales shorter than the ion-cyclotron period τ_c , the distribution function can be described by a beam. On the other hand, when the time scales are larger than τ_c , a ring distribution forms. A brief description of the linear instabilities driven by an ion beam streaming across a magnetic field in a plasma is presented. We have identified two types of instabilities occurring in low and high frequency bands; the low-frequency instability occurs over the frequency band from zero to about the lower-hybrid frequency for a sufficiently low beam density. As the beam density increases, the linear instability occurs at decreasing frequencies below the lower-hybrid frequency. The high frequency instability occurs near the electron cyclotron frequency and its harmonics. In the low earth orbit the low-frequency instability is likely to occur upto frequency $f < f_{th} \cong 5 \, kHz$. The electron cyclotron frequency in the ionosphere is about 1 MHz; thus an enhancement in the electric field noise upto a few MHz by the high frequency instability is expected. The wavelengths of the low frequency waves are found to range from a few tens of centimeters at relatively high plasma density ($\sim 10^6 cm^{-3}$) to a few meters at relatively low densities ($\sim 10^4 cm^{-3}$). The wavelength of the high frequency waves is just a few centimeters. In order to study the nonlinear evolution of the waves, we have performed 2.5-dimensional particle-in-cell (PIC) simulations which show that transient amplitudes of the waves can be upto a few *Volts / m* at the lower-hybrid frequency. The frequency spectrum of the waves from the simulation shows that the water ion beam

produces a broadband electric field noise extending in frequency upto a few times the ion plasma frequency. The simulations also reveal an enhanced electric field noise level near the electron cyclotron harmonics. The spectrum is characterized by a very low frequency peak below the lower-hybrid frequency, a relatively broad peak near it, and peaks near the first few electron cyclotron harmonics. The high frequency waves have not been measured from the shuttle, probably due to the long antenna used in the measurements.

2.5-dimensional simulations are computationally very expensive. Therefore, so far we have performed only a limited set of simulations which have not allowed us to reach a definite conclusion about the electric field levels in the different frequency bands. In order to reach a complete quantitative understanding of the effects of the contaminant ions on the space station's electromagnetic environment, we suggest that (1) further simulation studies be performed with realistic parameters of the ionosphere and (2) the high frequency response of the antenna used in the wave measurements aboard the space shuttle be further scrutinized to determine if the high frequency waves with wavelengths of a few tens of centimeters or shorter are artificially damped, causing a sharp roll-off in the frequency spectrum above about 10 kHz.

1. Introduction

Space shuttle flights have amply demonstrated that the contaminant gas plays an important role in determining the electromagnetic environment of a large spacecraft in the low earth orbit. In the case of the shuttle itself, water is the major contaminant [Paterson and Frank, 1989]. When water molecules undergo a charge-exchange with the oxygen ions, the major ion species in the ionosphere, a beam of H_2O^+ is created. Such ion beams traverse perpendicular to the geomagnetic field lines and interact with the ionospheric plasma to generate plasma waves, which contribute to the electromagnetic environment of the spacecraft.

The space station, as planned, is a large spacecraft and its electromagnetic environment is likely to be affected by the contaminants. In this report we present results from a study on the contributions of the contaminants to the electromagnetic environment of the space station, using appropriate linear theory for plasma instabilities and their numerical simulations.

A detailed summary of the measurements on the contaminant molecules and ions, and waves during some space shuttle flights can be found in a technical report by W. S. Kurth [1991], made to NASA Lewis Research Center. This report is a collection of papers in which measurements using the plasma diagnostic package (PDP) of the University of Iowa are reported and analyzed. Linear theories for the generation of plasma waves have been studied by Cairns and Gurnett [1990, 1991]. However, a linear instability theory cannot predict the saturated amplitude levels of the waves. In order to predict such amplitude levels, nonlinear theory and simulation studies are needed. The nonlinear processes also modify the frequency spectrum.

Recent studies show that observed waves are best described as wave modes driven by a water ion beam traveling with the orbital velocity of 8 *km/s*, perpendicular to the earth's magnetic field, in the ionospheric O^+ plasma [Cairns and Gurnett. 1991]. The excited mode is lower-hybrid waves. which propagate nearly perpendicular to the magnetic field. and have a wavelength approximately given by $\lambda = 2\pi / k \sim 2\pi V_{orb} / \omega_o$, where ω_o is the oxygen ion plasma frequency, and V_{orb} is the orbital velocity of the spacecraft. In low earth orbit the lower-hybrid frequency is about $f_{lh} \cong 5 kHz$, and for the ionospheric plasma density in the range

$10^{10} - 10^{12} m^{-3}$, the expected wavelength may range from about 10 cm to a few meters. The low-frequency instability for $f \leq f_{lh}$, driven by an ion beam traversing perpendicularly to the magnetic field, has been extensively studied in a laboratory plasma and a thorough discussion can be found in Seiler [1977].

In this study, we first perform a test particle study to determine the nature of the water ion velocity distribution function. We show that only on a time scale of the order of the ion-cyclotron period (τ_c) the distribution function becomes a ring if the water ions are continuously produced. In the spacecraft frame of reference, in which contaminants are released into the ionosphere, the center velocity of the ring is equal and opposite to that of the spacecraft velocity, the minimum velocity is zero and the maximum velocity is double that of the spacecraft velocity. The ring is created by the cycloidal motion of the contaminant ions in the crossed magnetic field and the convection electric field. At shorter time scales $t << \tau_c$, the ions are well described by a beam traversing perpendicular to the magnetic field in the ionospheric reference frame. *We perform a linear instability analysis for the beams showing that growing waves are possible in two separate frequency bands, a low-frequency band ranging from zero frequency to the lower-hybrid frequency in the plasma. The high-frequency band covers the electron cyclotron frequency and its harmonics, which fall in the megahertz range.* However, it turns out that for the ion beam velocity of 8 *km/s*, the growth rate for the excitation of the high frequency waves is about an order of magnitude smaller than that for the relatively low frequency waves near the lower-hybrid frequency. Therefore the high frequency waves may not grow to appreciable amplitudes.

We also present results from numerical simulations on the nonlinear evolution of the instabilities. Using a 2.5-dimensional particle-in-cell (PIC) code, we have simulated the generation of waves by an ion beam in a background plasma. Simulations reveal the excitation of both the low and high frequency instabilities. However, due to the artificial electron to ion mass ratio, the ion beam velocity used in the simulations becomes unrealistically high relative to the electron thermal velocity. Therefore, the high frequency waves are excessively enhanced compared to that expected for the orbital velocity of 8 *km/s* in the ionosphere. However, the low

4

frequency instability is correctly simulated and simulations predict a broadband excitation extending well above the lower-hybrid frequency; considerably enhanced electric field noise is found to occur at frequencies several times the ion plasma frequency. This suggests wave generation in the frequency range of a few hundred kilohertz in the ionosphere. In addition, the high frequency instability causes wave generation in the megahertz range. PIC simulations with realistic parameters of the ionosphere are expensive to run. Therefore, we have performed a limited set of simulations which correctly describe the linear and nonlinear evolution of the waves, but at this stage the results cannot be directly applied to the ionosphere. In order to reach a definite quantitative understanding of the waves, we have recommended further simulation studies using the code developed here, and further scrutiny of the wave measurements aboard the space shuttle, especially for the high frequency waves with short wavelengths.

2. Contaminant Ion Distribution Function

Before a study on wave generation by contaminant ions is made, it is essential to know the nature of the ion velocity distribution function. The basic problem is as follows. As the neutral contaminant atoms and/or molecules are released in the ionosphere, they move with the orbital velocity of the spacecraft with respect to the ionospheric plasma. After they undergo a charge exchange reaction with the ionospheric O^+ ions, the contaminants become ions and they are affected by the ambient magnetic field and the electric fields around the spacecraft. Since in the low earth orbit, a spacecraft charges to a negative potential less than 1 volt, the electric field effects associated with the charging are expected to be insignificant, and the earth's magnetic field determines the nature of the velocity distribution function. We performed calculations on the trajectories of a large number of H_2O^+ ions when they are suddenly released in a magnetic field of $B_o = 0.3 G$. The initial velocity distribution function of the ion cluster was assumed to be a Maxwellian with a temperature of 300°K. In the rest frame of the spacecraft, the ions also see the convection electric field given by $\underline{E} = \underline{V}_o \times \underline{B}_o$, where $\underline{V}_o$ is the spacecraft (orbital) velocity. Assuming $\underline{B}$ along the Z axis and $\underline{V}_o$ along the $-X$ axis, $\underline{E}$ is along the Y axis. The electric field causes an $\underline{E} \times \underline{B}_o$ drift in the X-direction, which is opposite to the velocity of the spacecraft. As the ions drift, their velocity distribution function changes in the $V_x - V_y$ plane as shown in Figure 1, which gives the location of the ion cluster in the $V_x - V_y$ plane at several selected times after their release. At the initial time $t = 0$, the average velocity of the ion cluster is zero. Due to the cyclotron motion, the trajectory of ions in the $V_x - V_y$ plane is a circle given by

$$V_x = \frac{E}{B_o}(1 + \cos\Omega_w t) \tag{1}$$

$$V_y = \frac{E}{B_o}\sin\Omega_w t \tag{2}$$

and the radius of the circle is $U = E_y / B_o$. In the above equations Ω_w is the water ion cyclotron frequency. In our calculations we measured time in units of Ω_o^{-1}, where Ω_o is the O^+ cyclotron frequency. The water ion cyclotron period is $\tau_{cw} = 2\pi/\Omega_w$ or $\tau_{cw}\Omega_o$

$= 2\pi\Omega_o / \Omega_w = 7.07$. The normalized time appearing in Figure 1 is defined by $\bar{t} = t\Omega_o$. For Figure 1, we assumed $U = 7.5 km/s$. The trajectory of the ions in Figure 1 agrees well with that given by equations (1) and (2). We note that if the ions were free to execute their cycloidal motion, their velocity range would be from zero to $2U$ in the spacecraft frame of reference. In the ionospheric reference frame the velocity ranges from $-U$ to U over a cyclotron period, with an average velocity of zero. Near the release time, the relative velocity of the ion cluster in the ionospheric reference frame is $-U$, which is relevant for the wave generation process, which is much faster than the ion gyration.

When the contaminant ions are created by charge exchange, they are created continuously. This continuous generation of ions modifies the distribution function significantly as shown in Figure 2. The ions progressively occupy a larger and larger portion of the circle shown in Figure 1 and described by equations (1) and (2), and in about one cyclotron period, the circle is completely populated giving a ring distribution in the $V_x - V_y$ plane. The thickness of the ring is determined by the initial thermal property of the ions.

The above results are based on test particle calculations, in which waves generated by the streaming ions are not included. In a later section we describe results from a self-consistent simulation showing how the waves begin to mix the ions in velocity space at a time shorter than a cyclotron period.

3. Linear Instability Analysis

We have identified two instabilities driven by an ion beam streaming perpendicular to the ambient magnetic field in a plasma. A low-frequency instability occurring for frequencies $f < f_{\ell h}$, where $f_{\ell h}$ is the lower-hybrid frequency, and a high-frequency instability for $f \cong n f_{ce}$, where f_{ce} is the electron-cyclotron frequency and $n = 1, 2, 3, \cdots$. We briefly describe the linear aspects of the instabilities here.

Low-Frequency Instability: Since the streaming ions excite waves at a time scale shorter than the ion-cyclotron period, it is useful to study linear wave excitation by an ion beam streaming perpendicular to the magnetic field. Assuming ions are cold and unmagnetized and electrons are highly magnetized, the dispersion relation for the angular frequencies $\omega << \Omega_e = 2\pi f_{ce}$ is given by

$$1 + \frac{k_x^2}{k^2} \frac{\omega_e^2}{\Omega_e^2} - \frac{\alpha \omega_i^2}{(\omega - k_x U)^2} - \frac{(1-\alpha)\omega_o^2}{\omega^2} - \frac{k_z^2}{k^2} \frac{\omega_e^2}{\omega^2} = 0 \tag{3}$$

where ω_e and ω_o are the electron plasma and O^+ ion plasma frequencies with the ambient plasma density N_o, respectively; ω_i is the contaminant ion plasma frequency with the density N_o; α is the contaminant ion relative beam density, i.e., $\alpha = n_w / N_o$ with n_i as the absolute density of the contaminant ions, k is the wave number with components k_z and k_x parallel and perpendicular to the ambient magnetic field, respectively; and U is the contaminant ion beam velocity along the x-direction. When the contaminant ions are H_2O^+, ω_i is denoted by ω_w, and n_i by n_w. When rearranged equation (3) becomes

$$P\tilde{\omega}^4 - 2\tilde{k}_x P\tilde{\omega}^3 + (P\tilde{k}_x^2 - \alpha m_o - Q) + 2\tilde{k}_x Q\tilde{\omega} - \tilde{k}_x Q = 0 \tag{4}$$

where,

$$P = 1 + y^2 \cos^2 \theta,$$

$$Q = 1 - \alpha + m_{oe} \sin^2 \theta,$$

$$y = \omega_e / \Omega_e, \quad \tilde{k}_x = k_x U / \omega_o, \quad \tilde{\omega} = \omega / \omega_o,$$

$$\tilde{m}_o = m_o / m_i, \quad m_{oe} = m_i / m_e$$

8

where m_0, m_i, and m_e are the mass of an oxygen ion, a contaminant ion and an electron, respectively; and θ is the angle between the wave vector k and a direction perpendicular to the magnetic field, i.e., $k_x = k \cos \theta$ and $k_z = k \sin \theta$.

For small α and $k_z = 0$, equation (3) can be solved analytically for the maximum growth rate and the corresponding wave frequency ω_r and wave number k_x. We seek solution for complex $\omega = \omega_r + i\gamma$ and obtain

$$k_x = (1-\alpha)^{1/2} \omega_{th} / U, \quad \omega_r = (1-\alpha)^{1/2} \omega_{th}(1-\delta_r), \quad \gamma = (1-\alpha)^{1/2} \omega_{th} \delta_i \qquad (5)$$

where ω_{th} is the lower-hybrid frequency, $\delta_r = 2^{-4/3}[\alpha/(1-\alpha)]^{1/3}$ and $\delta_i = \sqrt{3}\, \delta_r$. These solutions are written by analogy to the dispersion relation for the two-stream instability [Hasegawa, 1975].

We also solved equation (4) numerically and searched for complex roots $\tilde{\omega} = \tilde{\omega}_r + i\tilde{\gamma}$. The instability occurs when $\gamma > 0$. We have done this when the contaminant ions are water ions H_2O^+. Figure 3a shows the variation of $\tilde{\omega}_r = \text{Re}(\tilde{\omega})$ as a function of wave number $\tilde{k}_x$ for several values of the relative beam density α. The corresponding variation of the growth rate $\tilde{\gamma}$ is shown in Figure 3b. The plots in Figure 3a and 3b are for $\theta = 0$, i.e., for propagation perpendicular to the ambient magnetic field. For $\alpha = 0.1$, equation (5) yields results in reasonable agreement with a numerical results in Figures 3a and 3b. Note that for Figures 3a and 3b we assumed $\Omega_e / \omega_e = 1/3$.

We notice from Figures 3a and 3b that growing waves occur for $\tilde{k}_x \leq 0.6$, i.e., $k_x < 0.6\, \omega_o / U$. The growing waves are the slow beam mode as indicated by the fact that all curves in Figure 3a fall below the slant line given by $\omega = k_x U$ or $\tilde{\omega} = \tilde{k}_x$. As the beam density increases, the frequency of growing waves is seen to decrease, i.e., the wave frequency roughly scales with the plasma frequency of the stationary ion population. The frequencies of maximum growth rate are indicated by dots, one on each curve in Figure 3a. The lower-hybrid frequency given by $\omega_{th} \cong \sqrt{\Omega_e \Omega_i} = \omega_o / 3$ is indicated by an arrow on the ordinate of Figure 3a. We see

from this figure that, depending on the relative beam density the frequency of the maximum growth rate can occur at frequencies widely differing from the lower-hybrid frequency. Only for a sufficiently small beam density does the frequency of the maximum growth (ω_{max}) approaches $\omega_{\ell h}$. For example, when the beam density is 10% ($\alpha = 0.1$) and the stationary ion population is 90%, the maximum growth rate occurs at $\omega_r \approx \cdot 29\,\omega_o \sim \omega_{\ell h}$. As the beam becomes denser, ω_{max} decreases. When $\alpha = 0.9$, $\omega_{max} \cong .09\,\omega_o \cong 0.28\,\omega_{\ell h}$. Figure 3b shows that the maximum growth rate is obtained when $\alpha = 0.5$; as the relative beam density departs from this value, whether it increases or decreases, the growth rate decreases. It is also worth mentioning that the growth rates are approximately the same when the relative beam density is α or $1 - \alpha$

Figure 3b shows that the growing wave number is limited to $\bar{k}_{max} \lesssim 0.6$ or $k_x \lesssim 0.6\,\omega_o / U$. For the maximum plasma density of $10^6 cm^{-3}$ in the ionosphere, the maximum value of $\omega_o = 327\,krad/s$. For this maximum value of ω_o along with $U = 8\,km/s$, $k_x \lesssim 24\,m^{-1}$ or the wavelength $\lambda > 2\pi/k \cong 25 cm$. If the plasma density is lower, the wavelength becomes longer. For example if $n_o = 10^4 cm^{-3}$, $\lambda > 250 cm$. Since the ionospheric plasma density typically ranges from 10^4 to $10^6 cm^{-3}$, the wavelengths of the linear waves can range from a few tens of centimeters to a few meters.

Figures 3a and 3b are for $\theta = 0$. The variations of the wave frequency and the growth rate with θ are shown in Figures 4a and 4b, respectively. In these figures the curves are the plots of the frequency ($\bar{\omega}_r$) and the growth rate ($\bar{\gamma}$) at wave numbers where the latter ($\bar{\gamma}$) maximizes. Curves for $\theta > .01$ are not reliable because at such angles the Landau damping by electrons reduces the growth rates and we have ignored this damping in writing the dispersion relation in equation (3). It is worth noting that the range of frequency for the wave excitation is significantly enhanced when $\theta > 0$. For example, when $\alpha = 0.1$, the growing waves occur upto $\omega_r \cong 0.6\,\omega_o$ for the angles $\theta \lesssim 0.01\,rad$ compared to $\omega_r \cong 0.36\,\omega_o$ at $\theta = 0$.

High Frequency Instability: Besides the low frequency waves below the lower-hybrid frequency, there is a possibility of exciting high frequency waves at frequencies near $f = n f_{ce}$,

i.e., the harmonics of the electron-cyclotron frequency [Forslund et al, 1970]. The excited waves are the electron cyclotron waves described by the dispersion relation

$$(k_x \lambda_d)^2 = -1 + e^{-\lambda} I_0(\lambda) + 2\omega^2 \sum_{n=1}^{\infty} \frac{e^{-\lambda} I_n(\lambda)}{\omega^2 - (n\Omega_e)^2} + \frac{1}{2}\alpha Z'(\frac{\omega - k_x U}{k_x V_w}) + \frac{1-\alpha}{2} Z'(\frac{\omega}{k_x V_o}) \qquad (6)$$

where $\lambda = (k r_e)^2 / 2$, r_e is the electron Larmor radius given by $r_e = V_e / \Omega_e$, $I_n(\cdot)$ is the modified Bessel function of the first kind, λ_d is the plasma Debye length, and the terms containing Z' represent the contribution of ions to the dielectric function of the plasma. Z' is the first derivative of the plasma dispersion function [Fried and Conte, 1961]. The fourth term on the right hand side of equation (6) is the contribution from H_2O^+ ions and the argument of Z' in this term contains the Doppler-shifted frequency $\omega - k_x U$ divided by the product of k_x and the thermal velocity of the water ions V_w. Likewise, the fifth term is the contribution of oxygen ions. In the limit of small drift velocity, the real frequencies ω_r and growth rates γ of the waves are given by [Forslund et al, 1970]

$$\omega_r \cong n\Omega_e \qquad (7)$$

$$\gamma = \frac{n\Omega_e}{2\pi^{1/2}} \frac{1}{k r_e} \frac{Z'_{im}(\xi_r)}{[1 + (k\lambda_d)^2 - Z'_r(\xi_r)]^2} \qquad (8)$$

where

$$\xi_r = (\omega_r - kU) / kV_w, \quad Z'_{im}(\cdot) = Im(Z'(\cdot)), \quad Z'_r(\cdot) = Re(Z'(\cdot)) \qquad (9)$$

The growth rate maximizes when $Z'_{im}(\cdot)$ maximizes. Since $Z'_{im}(\xi_r) = -2\xi_r \pi^{1/2} e^{-\xi_r^2}$, which becomes maximum when $\xi_r = -1/\sqrt{2}$ and the maximum value of $Z'_{im}(\cdot) \cong 1.5$. The corresponding value of $Z'_r(\xi_r) \cong 0.53$. Combining these facts, we obtain

$$\frac{\gamma}{\Omega_e} \cong \frac{1.5n}{2\pi^{1/2}} \frac{1}{k r_e} \frac{1}{[1.5 + (k\lambda_d)^2]^2} \qquad (10)$$

The corresponding wave number k can be calculated from $(\omega - kU)/kV_w \cong -1/\sqrt{2}$ or $\omega = k(U + V_w/\sqrt{2})$. Since $U >> V_w$, $k \cong n\Omega_e / U$ or $k r_e \cong nV_e / U$, and the growth grate is given by

11

$$\frac{\gamma}{\Omega_e} = \frac{1.5}{2\pi^{1/2}} \frac{U}{V_e} \frac{1}{(1.5 + n^2 \frac{\Omega_e}{\omega_e^2} \frac{V_e^2}{U^2})^2} \tag{11}$$

Since $V_e >> U$ ($U = 8km/s$, and $V_e \cong 190km/s$ for $0.1eV$ electron temperature),

$$\frac{\gamma}{\Omega_e} \cong \frac{1}{n^4} \frac{1.5}{2\pi^{1/2}} (\frac{U}{V_e})^5 (\frac{\omega_e}{\Omega_e})^4 \tag{12}$$

From the foregoing expression for the growth rate it is clear that the wave excitation near the electron cyclotron frequency and its harmonics is favored by a large plasma density so that $\omega_e >> \Omega_e$. Assuming typical values of $U = 8km/s$ and $V_e = 190km/s$, $\gamma/\Omega_e \cong 5.3 \times 10^{-8} n^{-4} (\frac{\omega_e}{\Omega_e})^4$. In a relatively dense ionospheric plasma with a density of $10^6 cm^{-3}$, $\omega_e \cong 2\pi \times 9 \times 10^6 rad/s$, the cyclotron frequency $\Omega_e \cong 2\pi \times 8.7 \times 10^5 rad/s$ and the corresponding growth rate $r = 6 \times 10^{-4} \Omega_e$.

We found that the growth rate at low frequencies ($f < f_o$) is about $0.1\omega_o$, which is about an order of magnitude or more larger than the corresponding growth rate at the frequencies near the electron cyclotron frequency and its harmonics. Therefore, the low frequency waves should dominate in the ionosphere.

4. Numerical Simulation

Simulation Technique: In order to estimate the effects of nonlinearities on the frequency spectrum and the wave amplitudes, we have performed numerical simulations using a particle-in-cell (PIC) code. We performed 2.5-dimensional simulations as illustrated in Figure 5. The plasma is two-dimensional in the x-y plane; the ambient magnetic field is primarily along the z axis, but it has a tiny component in the x-y plane as well. The plasma particles are like rods of finite size [e.g., see Birdsall and Langdon, 1985]. Although the simulation is two-dimensional in the configuration space, in velocity space we include all the three velocity components, i.e., V_x, V_y and V_z. For this reason the simulation is called 2.5-dimensional. We solve the equation of motion of charged particles in given magnetic fields and electric fields determined by the solution of the Poisson equation given by

$$\frac{\partial^2 \varphi}{\partial x2} + \frac{\partial^2 \varphi}{\partial y2} = -\rho / \varepsilon_o \tag{13}$$

where φ is the electric potential, ε_o is the permittivity of free space, and ρ is the charge density determined by the plasma particles. We solve equation (13) subject to the periodic boundary conditions in both x and y directions. The numerical solution of equation (13) is implemented by the Fast-Fourier-Transform (FFT) method, a two-dimensional Fourier transform of equation (13) gives

$$\tilde{\varphi}(k_x, k_y) = \frac{1}{\varepsilon_o} \frac{\hat{\rho}(k_x, k_y)}{(k_x^2 + k_y^2)} \tag{14}$$

where k_x and k_y are the wave numbers associated with the variation of the potential along the x and y directions, respectively. First we perform a two-dimensional transform of $\rho(x, y)$ to obtain $\hat{\rho}(k_x, k_y)$ using a Fast-Fourier-Transform IMSL subroutine. The solution $\varphi(x, y)$ from $\tilde{\varphi}(k_x, k_y)$ is obtained by an inverse transform using the same subroutine.

The equation of motion of charged particles is given by

$$m_\alpha \frac{dV_\alpha}{dt} = q_\alpha(\underline{E} + \underline{V}_\alpha \times \underline{B}_o) \tag{15}$$

where m_α and q_α are the mass and charge of a charged particle of type α, V_α is its velocity, $\underline{E}$ is the electric field and $\underline{B}_o$ is the ambient magnetic field. In our model (Figure 5), $\underline{E} = a_x E_x + a_y E_y$, $\underline{B}_o = B_{xo} a_x + B_{yo} a_y + B_{zo} a_z$, and equation (15) can be written as

$$m_\alpha \frac{dV_{x\alpha}}{dt} = q_\alpha (E_x + V_y B_{zo} - V_z B_{yo}) \tag{16}$$

$$m_\alpha \frac{dV_{y\alpha}}{dt} = q_\alpha (E_y - V_x B_{zo} + V_z B_{xo}) \tag{17}$$

$$m_\alpha \frac{dV_{z\alpha}}{dt} = q_\alpha (V_x B_{yo} - V_y B_{xo}) \tag{18}$$

Equations (16) and (17) are advanced in time using the leap-frog technique [Morse, 1970]. Equation (18) is advanced by realizing that

$$\frac{d}{dt}(m_\alpha V_{z\alpha} - q_\alpha x B_{yo} + q_\alpha y B_{xo}) = 0 \tag{19}$$

or

$$m_\alpha V_{z\alpha} - q_\alpha x V_{yo} + q_\alpha y B_{xo} = \text{constant} \tag{20}$$

With the known initial velocity and position of a charged particle, its velocity component at later times is determined in terms of its $x(t)$ and $y(t)$ coordinates which are available by solving (16) and (17).

We use the following normalizations and definitions in our subsequent discussions: position $\bar{r} = (\underline{r}/\lambda_{do})$, time $\bar{t} = t\omega_e$, velocity $\underline{\bar{V}} = \underline{V}/V_e$, density $\bar{N} = N/N_o$, potential $\bar{\phi} = \phi/\phi_n$, and electric field $\underline{\bar{E}} = E/E_o$, where λ_{do}, ω_e, V_e and N_o are the Debye length, electron plasma frequency, electron thermal velocity and density in the initial unperturbed plasma, respectively; $\phi_n = k_B T_o/e$, $E_o = \phi_n/\lambda_{do}$, and T_o is the initial electron temperature in the plasma.

Figure 5 shows that the simulation system is gridded with grid spacings Δx and Δy in the x and y directions, respectively. The system size $L_x \times L_y$ and the grid spacings Δx and Δy were varied during the course of the simulation. However, a typical system size is $\bar{L}_x \times \bar{L}_y = 256 \times 128$ with $\Delta \bar{x} = 2$ and $\Delta \bar{y} = 2$.

Initially at time $t = 0$, total numbers of electrons and ions were loaded uniformly in the x-y plane. The total number (N_p) of electrons and ions in the system are equal and typically $N_p = 163840$, which gives 5 particles per Debye square. In the simulations, each particle represents a large number of real electrons or ions. We used two types of ions corresponding to the ambient O^+ ions in the ionosphere and the contaminant ions such as the water ions, which are produced by charge exchange between O^+ and H_2O. In the rest frame of the spacecraft, at the time of the charge exchange H_2O^+ ions are stationary while O^+ and electrons drift relative to the spacecraft. This relative motion generates waves, which we are trying to simulate here. We performed our simulation in the ionosphere reference frame, i.e., we assume that O^+ and electrons are stationary and H_2O^+ are moving.

The initial velocity distribution functions of the electrons and ions are given by

$$F_e = \frac{N_o}{(2\pi k_B T_{eo} / m_e)^{3/2}} \exp[-\tfrac{1}{2}m_e(V_x^2 + V_y^2 + V_z^2)/k_B T_o] \qquad (21)$$

$$F_w = \frac{n_w}{(2\pi k_B T_o / m_w)^{3/2}} \exp[-\tfrac{1}{2}m_w((V_x - U)^2 + V_y^2 + V_z^2)/k_B T_o] \qquad (22)$$

$$F_o = \frac{n_o}{(2\pi k_B T_o / m_o)^{3/2}} \exp[-\tfrac{1}{2}m_o(V_x^2 + V_y^2 + V_z^2)/k_B T_o] \qquad (23)$$

where T_o is the initial temperature of electrons, oxygen ions and water ions; m_e, m_o, and m_w are the corresponding masses of the charged particles, U is the drift velocity in the rest frame of the ionosphere, with respect to which the H_2O^+ ions drift. In the above expressions, k_B is the Boltzmann constant, N_o is the unperturbed density and the ion densities n_o and n_w are such that $N_o = n_o + n_w$.

Two-dimensional simulations with real masses of electrons and ions become prohibitively expensive. Therefore, we have performed simulations using artificial mass ratio; we have performed simulations with $m_o / m_e = 512$ and 2048 while keeping $m_o / m_w = 16/18$. The last ratio correctly reflects the ratio of oxygen ion mass to the water ion mass. The former ratios are chosen to be sufficiently large to adequately separate the electron and ion time scales. As we discuss later, the larger the mass ratio m_o / m_e the more realistic the simulation results become.

Typically in the ionosphere O^+ thermal velocity is about $V_o \cong 1 \, km/s$, electron thermal velocity $V_e \cong 190 \, km/s$, and the orbital velocity about $U \cong 8 \, km/s$. For the above reduced ion mass in the simulation, the thermal velocity of O^+ ions $V_o \cong (\frac{m_e}{m_o})^{1/2} V_{te}$, which is about an order of magnitude (or more) larger than the real value in space which is $V_o \cong 1/190 \, V_e = 0.0053 V_e$. Since for the low-frequency waves the ion dynamics is important in the present study, we keep the ion thermal and drift velocities in the same proportion as in the ionosphere, but then the drift velocity becomes a sizable fraction of the electron thermal velocity. For example, we present results from simulations with $m_o/m_e = 512$ and $U = 9 V_o \approx 0.4 V_e$, and also for much heavier ions with $m_o/m_e = 2048$ and $U = 0.2 V_e$. These choices of the drift velocity for the respective mass ratio correctly predict the low frequency behavior, but they also reveal enhanced electric field noise near the electron cyclotron frequency and its harmonics.

Numerical Results:

Before we begin to present numerical results, it is worthwhile to know some of the characteristic plasma frequencies in low earth orbit. Theses frequencies are summarized here as follows:

electron cyclotron frequency: $\qquad f_{ce} = \frac{1}{2\pi} \frac{eB_o}{m_e} = 0.87 \, MHz$

O^+ cyclotron frequency: $\qquad f_{co} = \frac{m_e}{m_i} f_{ce} \cong 30 \, Hz$

lower-hybrid frequency: $\qquad f_{lh} = \sqrt{f_{ce} f_{co}} \cong 5 \, kHz$

electron plasma frequency: $\qquad f_e = \frac{1}{2} \pi (\frac{n_o e^2}{m_e \varepsilon_o})^{1/2} \cong 1 - 9 \, MHz$

ion plasma frequency: $\qquad f_o = 5.2 - 52 \, kHz$

The cyclotron and the lower-hybrid frequencies are for a magnetic field $B_o = 0.3 \, G$. The values of f_e and f_o are based on plasma densities in the range $N_o = 10^4 - 10^6 \, cm^{-3}$. Comparing f_{ce} and f_e, we notice that $f_{ce}/f_e < 1$. In the simulation we typically chose $f_{ce}/f_e = 1$ and 0.3, which represent the situation in the wake region and outside it, respectively.

In our calculations lower-hybrid frequency is an important parameter; the value quoted above is approximate and its exact value is given by

$$f_{th} = \sqrt{f_{ce}f_{ci}} \; (\frac{f_o^2}{f_{ce}f_{ci} + f_o^2})^{1/2} \qquad (24)$$

When $f_{ce}f_{ci} << f_o^2$, $f_{th} \cong \sqrt{f_{ce}f_{ci}}$. On the other hand when the plasma density becomes sufficiently low making $f_{ce}f_{ci} >> f_o^2$, $f_{th} \cong f_o$; in the ionosphere this should happen when plasma density $N_o < 10^4 \, cm^{-3}$ and it is a distinct possibility inside the wake of a spacecraft.

With the artificial mass ratio $m_o / m_e = 512$, the ratios of some of the frequencies given above are modified as follows: $f_e / f_o = 22.6$ and not 171.4 like in the ionosphere, and similarly $f_{ce} / f_{co} = 512$ and not 2.9×10^4. Since ions play a crucial role in the low-frequency instability described here, the lowering of these ratios allows us to see the complete evolution of the instability in a comparatively short time. The lower-hybrid frequency in our simulation is given by

$$f_{th} = (\frac{m_e}{m_o})^{1/2} (\frac{f_{ce}}{f_e}) \; (1 + f_{ec}^2 / f_e^2)^{-1/2} f_e$$

For a typical ionospheric density of $N_o = 10^5 cm^{-3}$, $B_o = 0.3G$ and $m_o / m_e = 512$, $f_{ce} / f_e \cong 0.3$ and $f_{th} \cong 0.013 f_e$. When the mass ratio m_o / m_e is increased to 2048, $f_{th} = 0.067 f_e$. When the plasma density is reduced, like in the wake region of a spacecraft, the ratio f_{th} / f_e is increased; for example if $N_o = 10^4 cm^{-3}$, $f_{ce} / f_c \cong 1$ and $f_{th} / f_e \cong 0.03$ for $m_o / m_e = 512$.

Simulation with $m_o / m_e = 512$, $U / V_e = 0.4$ and $f_{ce} / f_e = 1$:

This simulation was performed to check some of the linear features of the waves as described in section 3. We performed the simulation for $f_{ce} / f_e = 1$, which is the case in the very low density region of the wake. As noted above, this gives $f_{th} \cong 0.03 f_e$. We performed simulations with $n_w / N_o = 0.1$, $T_o = T_w = T_e = T_o$ and $U / V_e = 0.4$. One may wonder why such large drifts in terms of electron thermal velocity are chosen. As explained earlier, for the artificial mass ratio $m_o / m_e = 512$, the ratio of O^+ thermal velocity to that of the electrons is $V_o / V_e = 0.045$ and not 0.006 as for the real mass ratio of $m_o / m_e = 29376$. In order to

properly treat the low frequency waves, for which ion dynamics is crucial, we keep the ion Mach number, i.e., $M = U/V_o$ as close as possible to that in low earth orbit. The choice of $U/V_e = 0.4$ gives $M = 9$ which is close to that given by a drift velocity of 8 km/s.

Figure 6 shows the temporal evolution of the wave; in Figure 6a we have plotted the normalized electric potential $\tilde{\phi}$ at the center of the simulation region, i.e., at the point (128,64). Figures 6b and 6c show the electric fields $\tilde{E}_x$ and $\tilde{E}_y$ at the same point, respectively. These figures clearly show that the waves grow and then they decay. It is also apparent that the waves have low and high frequency components. From Figure 6a, we find that the dominant low frequency component has a time period $\tau_\ell \cong 260\,\omega_e^{-1}$, which gives a frequency $f = \tau_e^{-1} \cong (2\pi/260)f_e = 0.024\,f_e$, which is slightly lower than the lower-hybrid frequency mentioned above. We saw in section 2 that for sufficiently low beam density, the strongest growing waves have frequencies close to the lower-hybrid frequency (see Figures 3a and 3b).

The maximum amplitude of the electric field is about $0.25kT_o/e\lambda_d$. For $kT_o = 0.2eV$ and $\lambda_d = 3.4cm$ for a plasma density $N_o = 10^4\,cm^{-3}$, the maximum electric field $E \cong (E_x^2 + E_y^2)^{1/2} \approx \sqrt{2} \times 0.25 \times 0.2/.034 = 2V/m$. Thus in response to the injection of water and its subsequent charge exchange, transient fields of a few Volts/meter are expected, which is in contrast to the average rms fields of about a few multivolts/m measured from the shuttle [Gurnett et al, 1988].

From the electric potential and the fields, one can estimate the wave number and wavelength of the waves. Since $\underline{E} \sim \underline{k}\phi$, where $\underline{k} = k_x\hat{a}_x + k_y\hat{a}_y$, we estimate that a typical value of $\bar{k}_x$ for the low frequency wave is $\bar{k}_x = \tilde{E}_x/\tilde{\phi} \approx 0.7$, which yields a wavelength $\lambda_x = \frac{2\pi}{k_x} = (2\pi/0.0)\lambda_d = 89\,\lambda_d$. The linear solution for the waves in equation (5) yields $k_x \cong 0.066\,\lambda_d^{-1}$ and $\lambda_x = 95\,\lambda_d$. Thus the wave number from the simulation is seen to agree with the linear solution.

The frequency spectrum of the electric fields shown in Figure 6 is plotted in Figure 7. There are two curves in this figure. The solid curve is obtained by performing Fourier transform of the data plotted in Figures 6b and 6c; the data analyzed is obtained by calculating

18

$E = (E_x^2 + E_y^2)^{1/2}$. The broken-line curve is the noise in the simulation when the drift velocity

$U = 0$. We notice that the spectrum is considerably enhanced over the noise level in two

frequency bands; the low frequency band is $f \leq 0.1 f_e$, which in our simulation is about

$2 f_o$, where f_o is the ion plasma frequency. The high frequency band consists of the sharp

peaks near the electron cyclotron harmonics. These enhancements are expected from the linear

instability analysis presented in section 2.

The low frequency band has its own structures. We see a strong enhancement near the

lower-hybrid frequency which in our simulation is $0.03 f_e$. We also see a strong enhancement at

very low frequencies $f \leq 0.01 f_e$. The peak near the lower-hybrid frequency is expected from the

linear instability analysis presented in section 3; but we see that it is considerably broadened, and

the enhancement extends to higher frequencies upto twice the ion-plasma frequency. The

enhancement at very low frequency represents the temporal modulation of the wave amplitude

shown in Figures 6a, 6b, and 6c; this modulation consists of the initial stage of the wave growth

followed by its saturation and eventual decay.

In the simulation described above we have used a relatively low artificial mass ratio of

$m_o / m_e = 512$, which reduces the ion cyclotron period. Thus, as the ions excite the wave they are

significantly affected by their cyclotron motion. This is shown in Figure 8, which displays the

evolution of the ions in the $V_x - V_y$ velocity space as the instability develops (Figure 6). Water

ions are injected at $t = 0$ with a drift velocity $U = 0.4 V_e$ along the x direction.

The ion cyclotron period in the simulation for water ions is

$\tau_c \cong 2\pi / \Omega_\omega = 2\pi (m_\omega / m_e) / \Omega_e$. Since $\Omega_e = \omega_{pe}$ in the simulation described here,

$\bar{\tau}_c = \tau_c \omega_{pe} = 2\pi (m_{\omega+} / m_e) = 3619$. This cyclotron period is clearly visible from the rotation of

the water ions around the oxygen ions in the $V_x - V_y$ plane. We saw a similar rotation in Figure

1. The cyclotron motion shown in Figure 8 modulates the waves contributing to the very low

frequency peak in the frequency spectrum in Figure 7. In reality the normalized cyclotron period

is considerable larger and the mixing of water and oxygen ions as seen in Figure 8 for $\bar{t} \geq 2000$

occurs at a much shorter time scale relative to the cyclotron period. Thus the modulation due to

the cyclotron motion may not produce as low frequency as the ion cyclotron frequency, but a low frequency component is expected.

Simulation with $m_o / m_e = 2048$, $U / V_e = 0.2$ **and** $f_{ce} / f_e = 0.3$:

The simulation with the mass ratio of 2048 is more realistic, but we are still away from the real mass ratio by a factor of 14.3. Due to constraints on computer resources, so far we have not done the simulation with the real mass. Figure 9 shows the temporal evolution of the waves seen in the simulation. In this simulation, we used $n_o = n_w = 0.5 N_o$. Like in Figure 6, Figure 9a shows the evolution of the potential at the center point of the simulation region, while Figures 9b and 9c show the evolution of $\tilde{E}_x$ and $\tilde{E}_y$ at the same point. Note that the wave is seen to grow to a maximum amplitude of $|\phi| \cong 4 kT_o / e$ and the corresponding electric fields E_x and E_y have amplitudes upto about $0.15 kT_o / e\lambda_d$. For $kT_o = 0.2 eV$ and $\lambda_d = 1 cm$, the maximum electric field seen from this simulation is $E \approx (E_x^2 + E_y^2)^{1/2} = \sqrt{2} \times 0.15 \times .2 / 0.01 = 5 V / m$, which is somewhat larger than that seen from the previous simulation. The frequency spectrum of the waves shown in Figure 9 is plotted in Figure 10. Note that in this simulation $f_{ce} / f_e = 0.3$ and the O^+ ion plasma frequency is $f_o = 0.022 f_e$. The broken-line curve in Figure 10 is the background noise of the simulation when $U = 0$. The solid-line curve gives the frequency spectrum of the electric field data for $E = (E_x^2 + E_y^2)^{1/2}$ shown in Figure 9. The most dominant peak in the spectrum occurs below the lower-hybrid frequency. The enhancement in wave power over the background noise by an order of magnitude or more occurs upto a frequency $f = 0.1 f_e$ which is about $5 f_o$. Figure 10 also shows the high frequency waves near $f \sim 0.3 f_e$, $0.6 f_e$ and $0.9 f_e$, which are the harmonics of the cyclotron frequency $f_{ce} = 0.3 f_e$.

The evolution of the ion phase space in the $V_x - V_y$ plane is shown in Figure 11. In the present simulation which we are discussing here, the ion cyclotron period $\bar{\tau}_c = 42892$. Figure 11 shows that the water ions with the initial drift velocity of $U = 0.2 V_{ie}$ begin to gyrate as seen from the plots at $\bar{t} = 0$, 2000 and 4000. However, the waves act on them and they mix with the O^+ ions. The mixing has begun at $\bar{t} = 4000$ and by the end of the simulation at $\bar{t} = 9000$

20

the two types of ions have undergone a considerable mixing in the $V_x - V_y$ velocity space. This feature of the present simulation with mass ratio of $m_o / m_e = 2048$ and $f_{ce} / f_e = 0.3$ is quite different from that shown in Figure 8 from the simulation with $m_o / m_e = 512$ and $f_{ce} / f_e = 1$. The mixing of the ions in the $X - V_x$ phase space is shown in Figure 12. At the initial time we note the O^+ ions have zero average drift velocity while the water ions have an average drift $\bar{U} = 0.2$. Figure 12a shows that at $\bar{t} = 1500$, there is only a weak perturbation in the phase space. As the waves intensify (Figure 9), the two ion populations undergo a coupling through the electric fields of the wave. As seen from Figure 12b, vortices appear by the time $\bar{t} = 3500$ and they fill up progressively mixing the O^+ and H_2O^+ ions.

The ion distribution in the $V_x - V_y$ plane shown in Figure 11f is a pancake type as observed from the space shuttle [Paterson et al, 1989]. However, the distribution shown in this figure is in the frame of the reference of the ionospheric plasma in which O^+ ions are stationary while the H_2O^+ ions drift with the shuttle speed. The waves modify the distribution functions of both oxygen and water ions in the plane perpendicular to the magnetic field. Figures 13a and 13b show the parallel velocity distribution function $F(V_z)$ of O^+ and H_2O^+, respectively. Over the simulation time of $\bar{t} = 9000$, O^+ ions show hardly any change in $F(V_z)$, while H_2O^+ ions show a slight modification; these ions gain a slight drift along the z direction due to the $V_y \times B_x$ force acting on them. Figures 13c and 13d show $F(V_x)$ and $F(V_y)$ for the O^+ ions, respectively. The O^+ ions are seen to develop nearly a symmetric tail in V_x which amounts to the ion heating. The O^+ ions are seen to develop an asymmetric tail along $-V_y$. This is connected with the cyclotron motion of H_2O^+ ions and the interaction between O^+ and H_2O^+ ions through the waves. Figures 13e and 13f show the $F(V_x)$ and $F(V_y)$ for the H_2O^+ ions, respectively. It is seen that the H_2O^+ ions loose their initial drift along X to that along V_y due to the cyclotron motion. It should be also pointed out that partly the loss of the momentum, i.e., reduction in V_x must be due to the wave generation. Besides the transfer of drift motion from V_x to V_y, it is also seen that the water ions are heated as evidenced by the increase in the velocity spread of the distribution shown in Figures 13e and 13f with increasing time.

21

The electron distribution functions corresponding to those of ions in Figure 13 are shown in Figure 14. Figures 14a, 14b and 14c show $F(V_x)$, $F(V_y)$ and $F(V_z)$, respectively. These figures shown only slight heating in V_x and V_y. On the other hand, the heating in V_z is appreciable. The electron and ion heatings seen here are similar to those reported by McBride [1972], who studied the generation of the lower-hybrid waves in a plasma where the entire ion population drifted across the ambient magnetic field.

5. Conclusions and Discussions

We have performed a systematic study of the wave generation by contaminant ions near a large spacecraft in low earth orbit. Our study includes (1) test particle simulation on the contaminant ion velocity distribution function, (2) linear wave analysis, and (3) self-consistent numerical simulation of the wave generation by the contaminant ion beam traversing perpendicular to the electric field.

The test particle simulation revealed that for short time scales at which the waves are generated the contaminant ions can very well be represented by an ion beam rather than a ring, which forms at the time scale of the ion cyclotron period. The self-consistent 2.5-D numerical simulations with large ion to electron mass ratio corroborate the above statement.

The linear instability analysis revealed that the waves occur in two frequency bands: (1) a low frequency band for $f \leq f_{th}$, and (2) a high frequency band with $f = n f_{ce}$, where f_{ce} is the electron cyclotron frequency and $n = 1, 2, 3, \cdots$. Comparing the growth rates of the waves in the two frequency bands for a contaminant ion beam velocity of $U = 8 \, km/s$, it turns out that the waves in the high frequency band may not be appreciably amplified because $U << V_{te}$, the electron thermal velocity. In view of our simulation with a relatively large mass ratio, for which the high frequency waves remain significantly amplified (Figure 10), the amplification needs to be firmly established by further simulations as we discuss later.

The self-consistent 2.5-D simulations do show that the lower-hybrid waves are excited along with the high frequency waves. The low frequency waves can have wave amplitudes upto a few *Volts/m* depending on the relative densities of the contaminant and oxygen ions. Simulations show that the wavelength of the low frequency waves is in agreement with that found from the linear instability analysis.

In contrast to the linear-instability analysis, the 2.5-D simulations show low-frequency wave excitation in a broad frequency band, not limited to $f < f_{th}$, but extending to frequencies several times the O^+ ion plasma frequency. The extension of the low frequency waves above the

23

lower-hybrid frequency is not predicted by the linear instability analysis; it is a consequence of nonlinear plasma processes.

The low frequency waves at frequencies $f < 30\,kHz$ are not relevant to the space station's electromagnetic environment. In low earth orbit the lower-hybrid frequency is about $5\,kHz$ and the oxygen plasma frequency f_o can range from 5 to $50\,kHz$ as the plasma density ranges from 10^4 to $10^6 cm^{-3}$. If the nonlinearly generated low frequency waves extend in frequency upto several times f_o, it is distinctly possible that waves in the frequency range upto a few hundred kHz are generated. The observations from the space shuttle show waves extending to $50\,kHz$. However, the measured frequency spectrum (see Figure 15) shows that the wave power sharply falls off at frequencies above the lower-hybrid frequency [Cairns et al, 1991]. It is worth pointing out that with increasing wave frequency the wavelength get shorter and shorter, making wave measurements with a relatively long antenna rather inaccurate; the antenna response may attenuate the measured waves. The IOWA PDP instrumentation carried a 3.9-m long antenna [Gurnett et al, 1988], which could not correctly measure waves having wavelengths shorter than a few tens of centimeters.

The comments made above also hold good for the high frequency waves near $f = n f_{ce}$. The wavelengths at such frequencies are shorter than the electron gyro-radius which is about 3 cm in low earth orbit. Waves with such short wavelengths are difficult to measure with an antenna of a few meters in length. Comparing Figures 10 and 15, we note that the simulated and measured spectra have some similarities, at least for frequencies $f < 30\,kHz$. The difference at higher frequencies is due to simulational inadequacies or due to the error in the measurements. At this juncture we are not sure about the real cause of the difference.

Recommendations:

Under the present grant, we have developed the analytic capability to predict the entire frequency spectrum of the waves generated. The main tool we developed is the 2.5-dimensional PIC code. So far we have ~~done simulations~~ with only 5 particles per Debye cell, which is too

small and it gives enhanced plasma fluctuations even without the wave generation. The background noise in Figures 7 and 10 are the consequence of this limited number of particles in the simulation. So far our simulation is also limited in terms of ion to electron mass ratio; we have used $m_o/m_e = 2048$, which is smaller than the real mass ratio of m_o/m_e by a factor of about 14.3. The use of artificial mass ratio is required for the purpose of the computational economy. The run with the mass ratio 2048 used 18 hours of CPU on a VAX 7000 machine. The use of the artificial mass ratio also necessitates that the drift velocity of the water ions be relatively large in terms of electron thermal velocity. This enhances the wave generation at the electron cyclotron frequency and its harmonics.

We recommend that a few simulations be performed with the real parameters of the problem, and with a sufficiently large number of particles that the background noise is sufficiently suppressed. Such simulations along with further scrutiny of the measured wave data in terms of antenna response for correctly measuring the short wavelength (high frequency) waves are essential for a full understanding of the effects of the contaminant ions on the electromagnetic wave environment of the space station.

The low frequency waves with frequencies upto a few tens of kilohertz do not appear to be of much concern for the space station. But the high frequency waves in the MHz range near the electron cyclotron frequency and its harmonics may be of concern. These waves are extremely short wavelength waves. We feel that the PDP measurements at such high frequencies may not be correct due to the antenna response. Further simulations, as suggested above, may prove to be useful.

References

Birdsall, C. K., and A. B. Langdon, *Plasma Physics via Computer Simulation*, McGraw-Hill Book Company, New York, 1985.

Cairns, I. H., and D. A. Gurnett, Control of plasma waves associated with the space shuttle by the angle between the orbit's velocity vector and the magnetic field, *J. Geophys. Res.*, *96*, 7591, 1991.

Cairns, I. H., and D. A. Gurnett, Plasma waves associated with the space shuttle, *ESA sp-311*, 87, 1990.

Forslund, D. W., R. L. Morse, and C. W. Nelson, Electron cyclotron drift instability, *Phys. Rev. Lett.*, *25*, 1266, 1970.

Fried, B. D., and S. D. Conte, *The Plasma Dispersion Function*, Academic Press, New York, 1961.

Gurnett, D. A., W. S. Kurth, J. T. Steinberg, and S. D. Shawhan, Plasma turbulence around the shuttle: Results from the spacelab-2 flight, *Geophys. Res. Lett*, *15*, 760, 1988.

Hasegawa, A., *Plasma Instability and Nonlinear Effects*, Springer-Verlag, Berlin, Chapter 4, p. 160, 1975.

Kurth, W. S., Interpretation of plasma diagnostic package results in terms of large structure plasma interactions, *Final Tech. Report*, *NASA-Lewis Res. Center Grant*, *NAG3-449*, August 1991.

Morse, R. L., Multidimensional plasma simulations by particle-in-cell methods, in *Computational Physics*, edited by Alder, Feinback and Rotenberg, Academic Press, New York, pp. 1213-1239, 1970.

Paterson, W. R., and A. Frank, Hot ions plasma from the cloud of neutral gasses surrounding the space shuttle, *J. Geophys. Res.*, *94*, 3721, 1989.

Seiler, S. W., Linear and nonlinear development of a lower-hybrid wave driven by a perpendicular ion beam, *Ph.D. Thesis*, Princeton University, 1977.

26
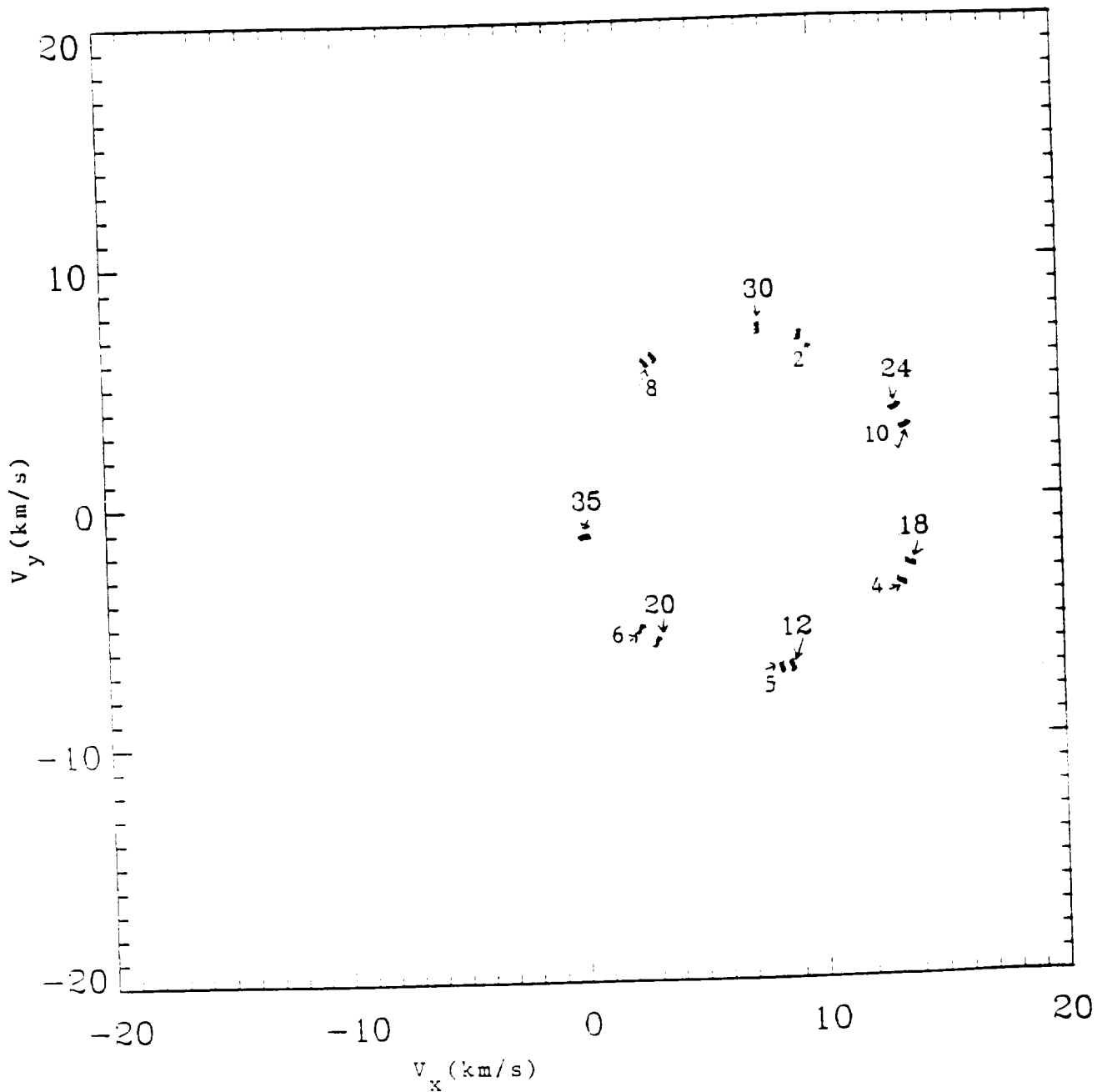
Figure 1. Water ion bunch gyrating in the $V_x - V_y$ plane when the magnetic field is in the z direction. Each bunch has 100 water ions. The numbers indicated by arrows are times in units of Ω_o^{-1} where Ω_o is the O^+ ion cyclotron frequency. The H_2O^+ cyclotron period is $\tau_{cw} = 7.07\,\Omega_o^{-1}$. Ions were followed for $\bar{t} = 35\,\Omega_o^{-1}$. The bunch always falls on a circle described by equations (1) and (2).
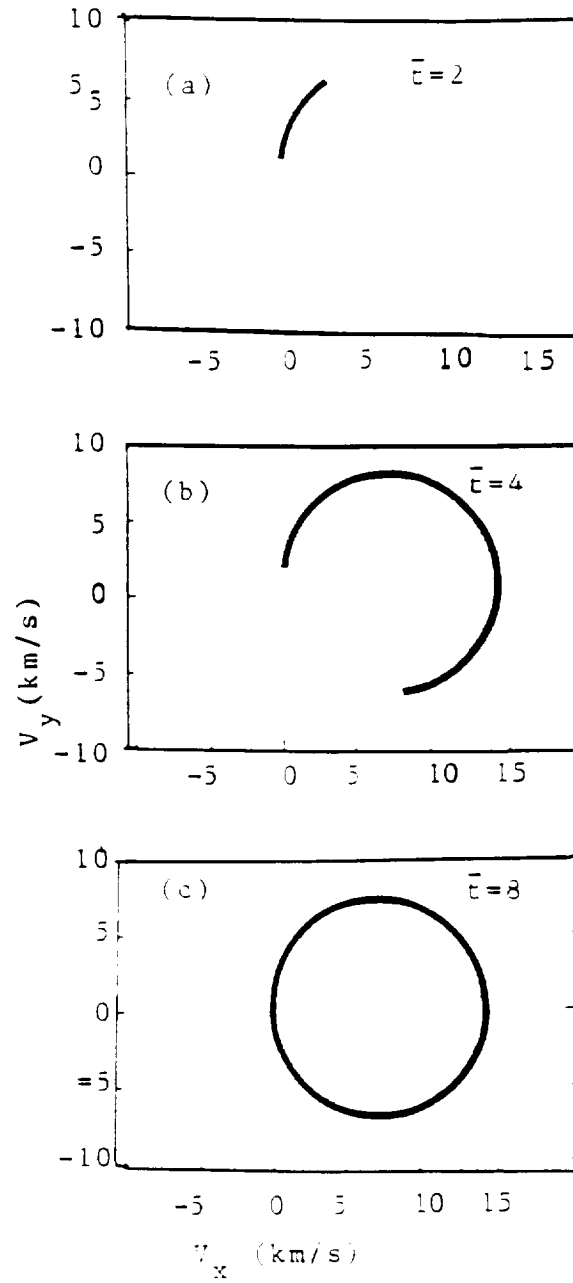
Figure 2. Ions' trajectory in the $V_x - V_y$ plane when they are continuously injected. (a) $t = 2 \, \Omega_o^{-1}$, (b) $t = 4 \, \Omega_o^{-1}$ and (c) $t = 8 \, \Omega_o^{-1}$. Note that with continuing injection of ions the beam arc at early times evolves in a ring distribution.
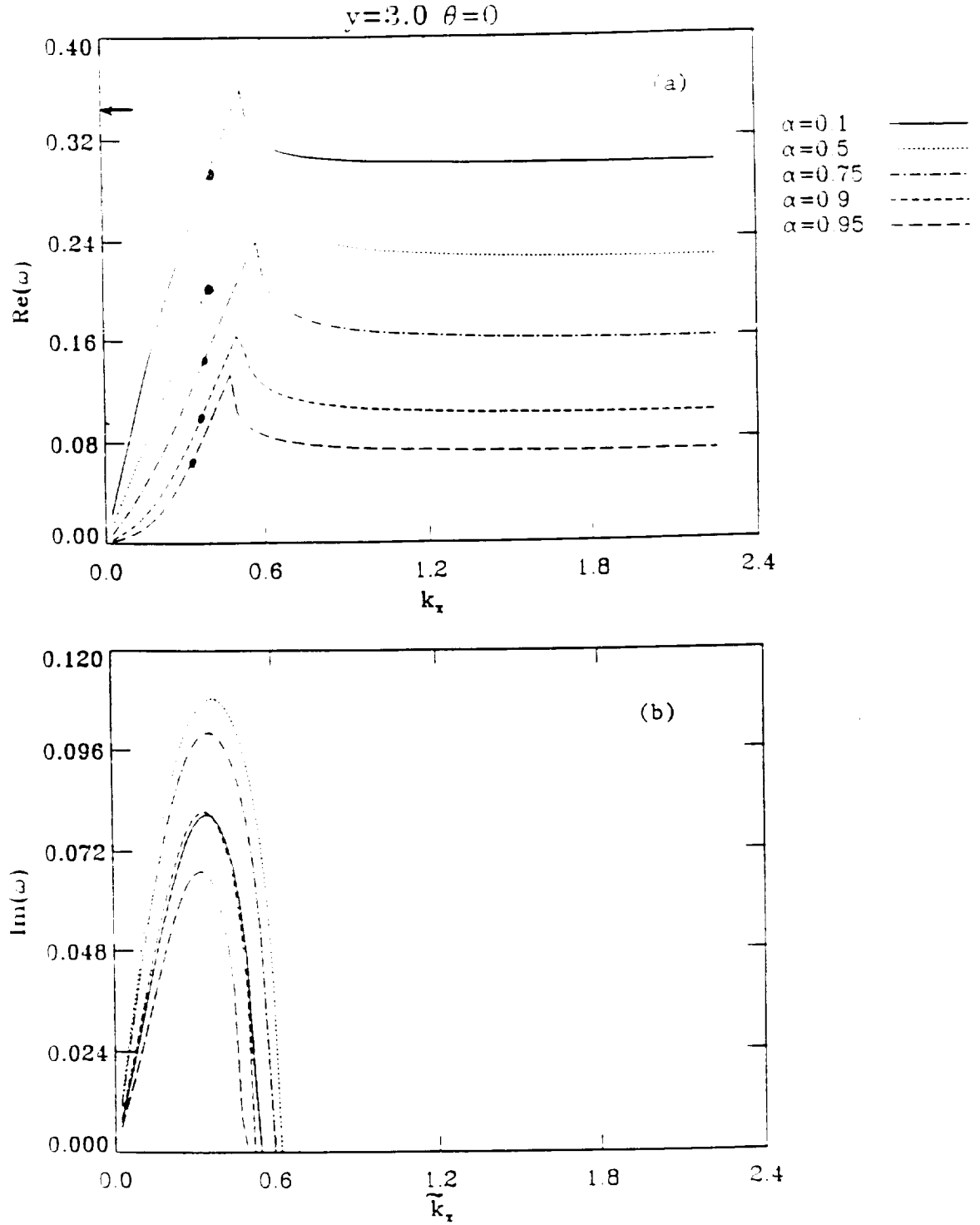
Figure 3. Results from linear instability analysis. (a) Wave frequency $\omega_r = R_e(\omega)$ as a function of wave number $\bar{k}_x$. Note that ω_o is in units of the oxygen ion plasma frequency determined by the density in the ambient plasma without the water ions. (b) Growth rate is in units of ω_o. the several curves in (a) and (b) are for different values of the water ions relative density given by α in the legend. Other parameters for this figure are $\theta = 0$ and $\omega_e / \Omega_e = 3$.
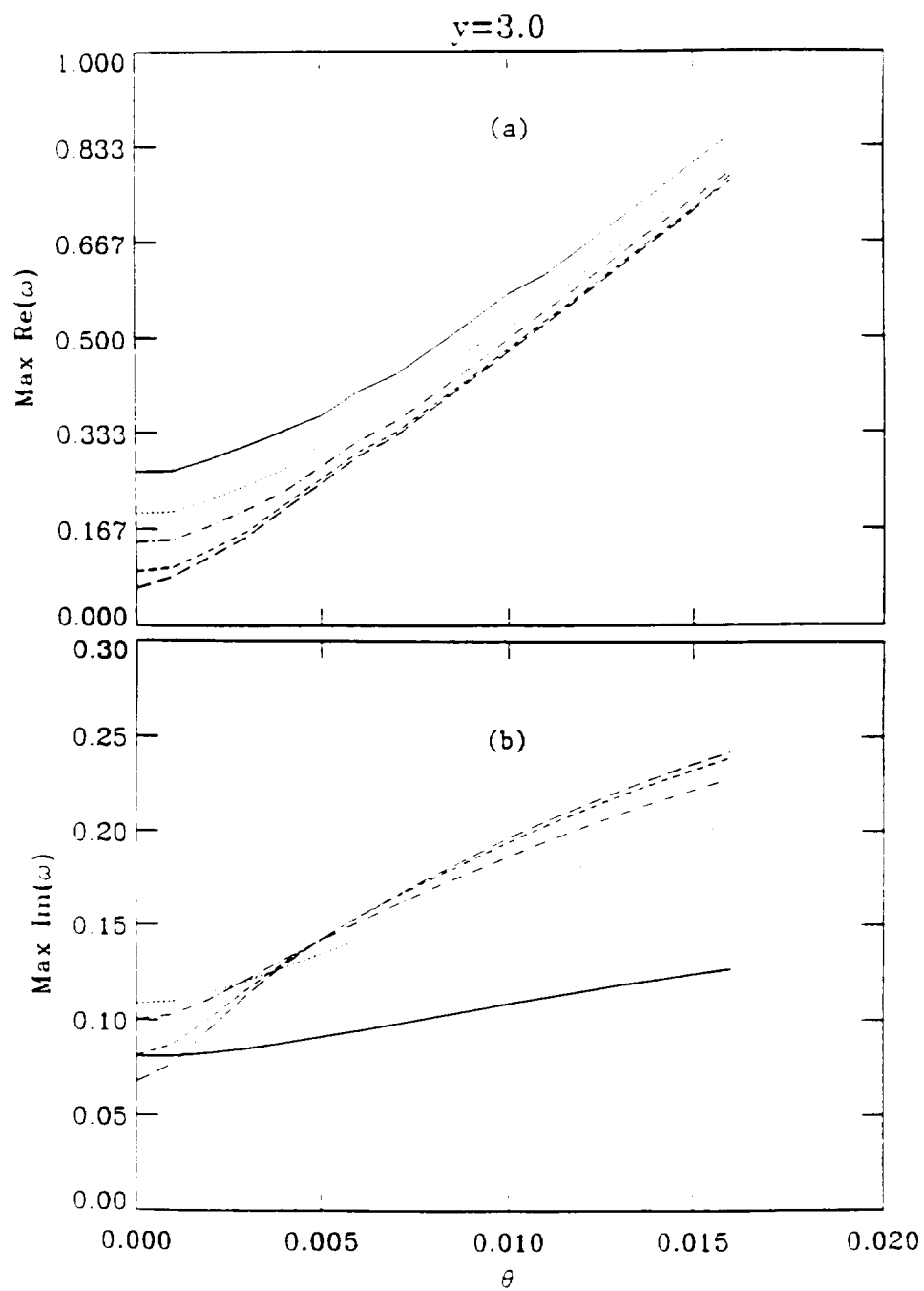
Figure 4. (a) Plots of frequencies at which maximum growth rate occurs versus θ for different values of α. (b) Plots of maximum growth rate versus θ for different values of α.
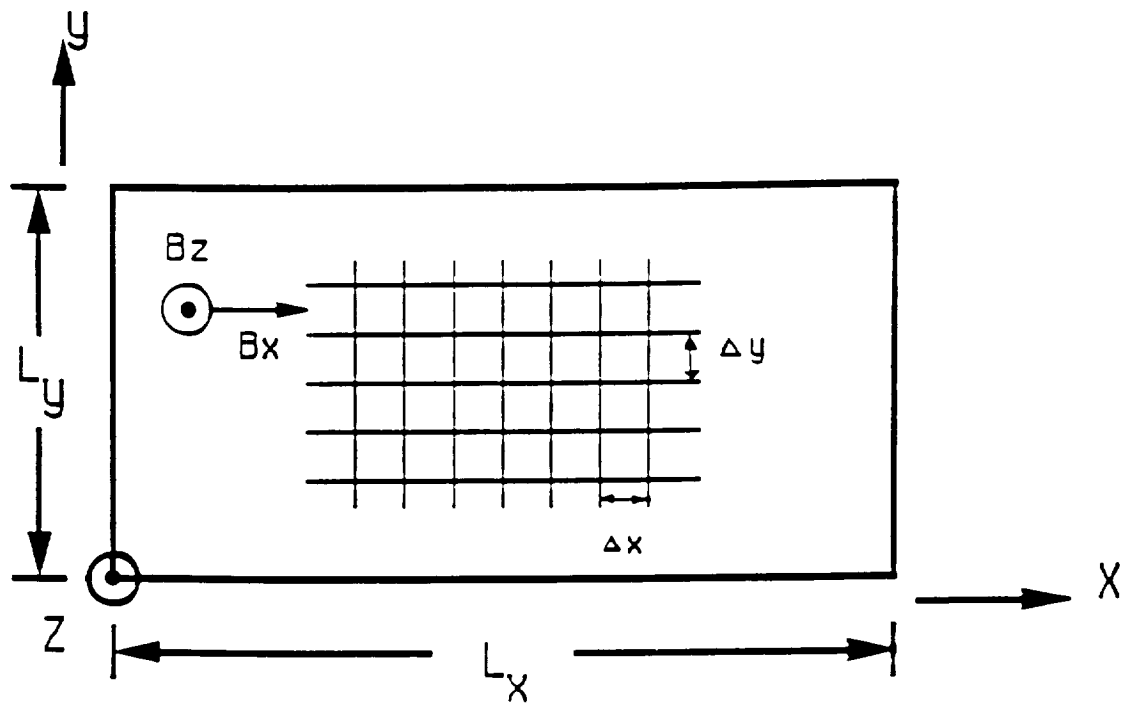
Figure 5. Geometry of the 2 1/2-dimensional simulation. Simulation is performed in the x-y plane. The dominant component of the magnetic field is in the z direction. A tiny component of the magnetic field is in the x-y plane; in the simulations described here this component is along the x direction.
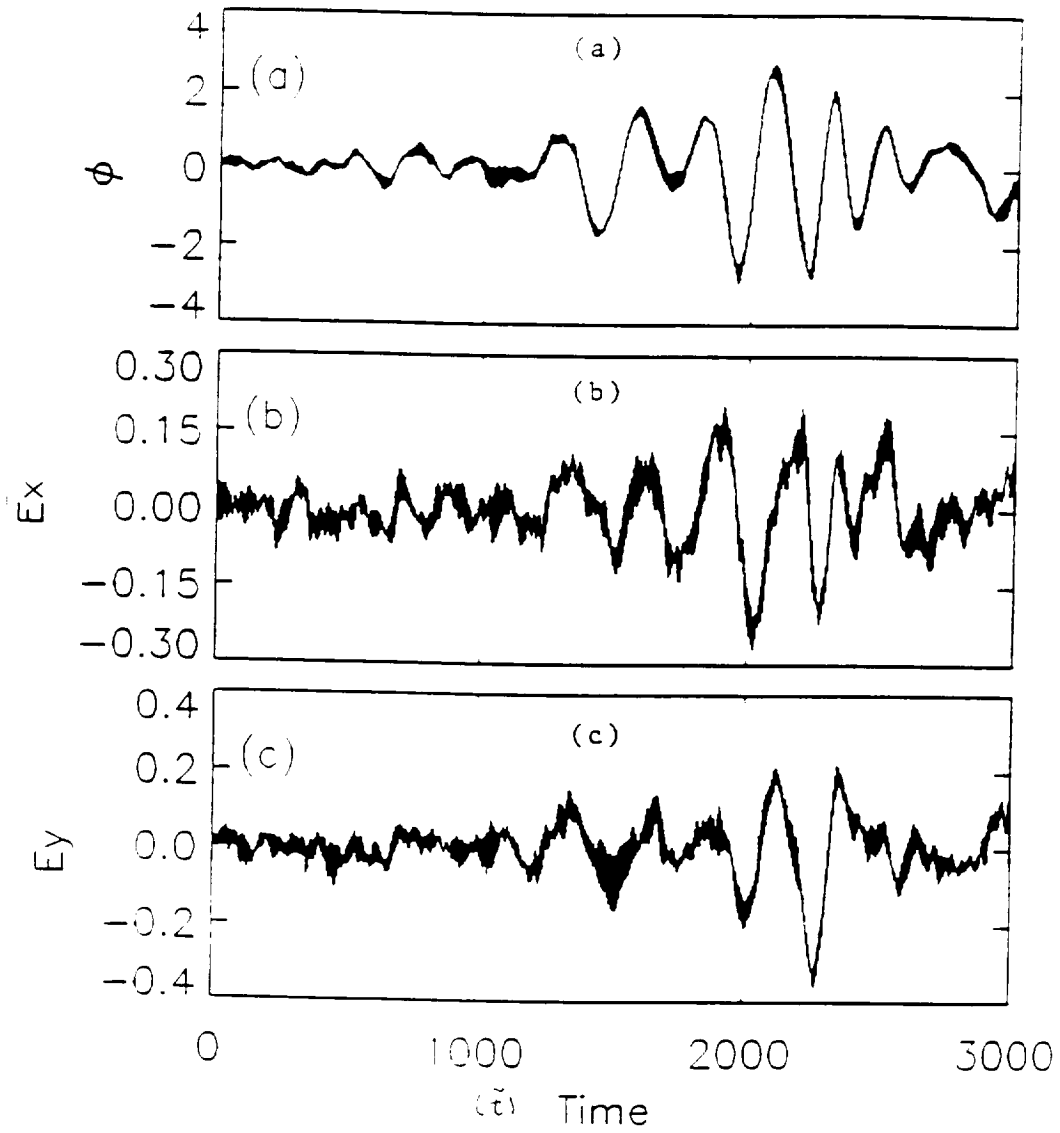
Figure 6. Temporal evolution of (a) normalized potential $\tilde{\Phi}$, (b) normalized electric field $\tilde{E}_x$ and (c) $\tilde{E}_y$. The horizontal axis is normalized time $\bar{t} = t\,\omega_e$. For this run $\Omega_e = \omega_e$, $n_w = 0.1\,N_o$, $m_i/m_e = 512$, and $U/V_e = 0.4$.
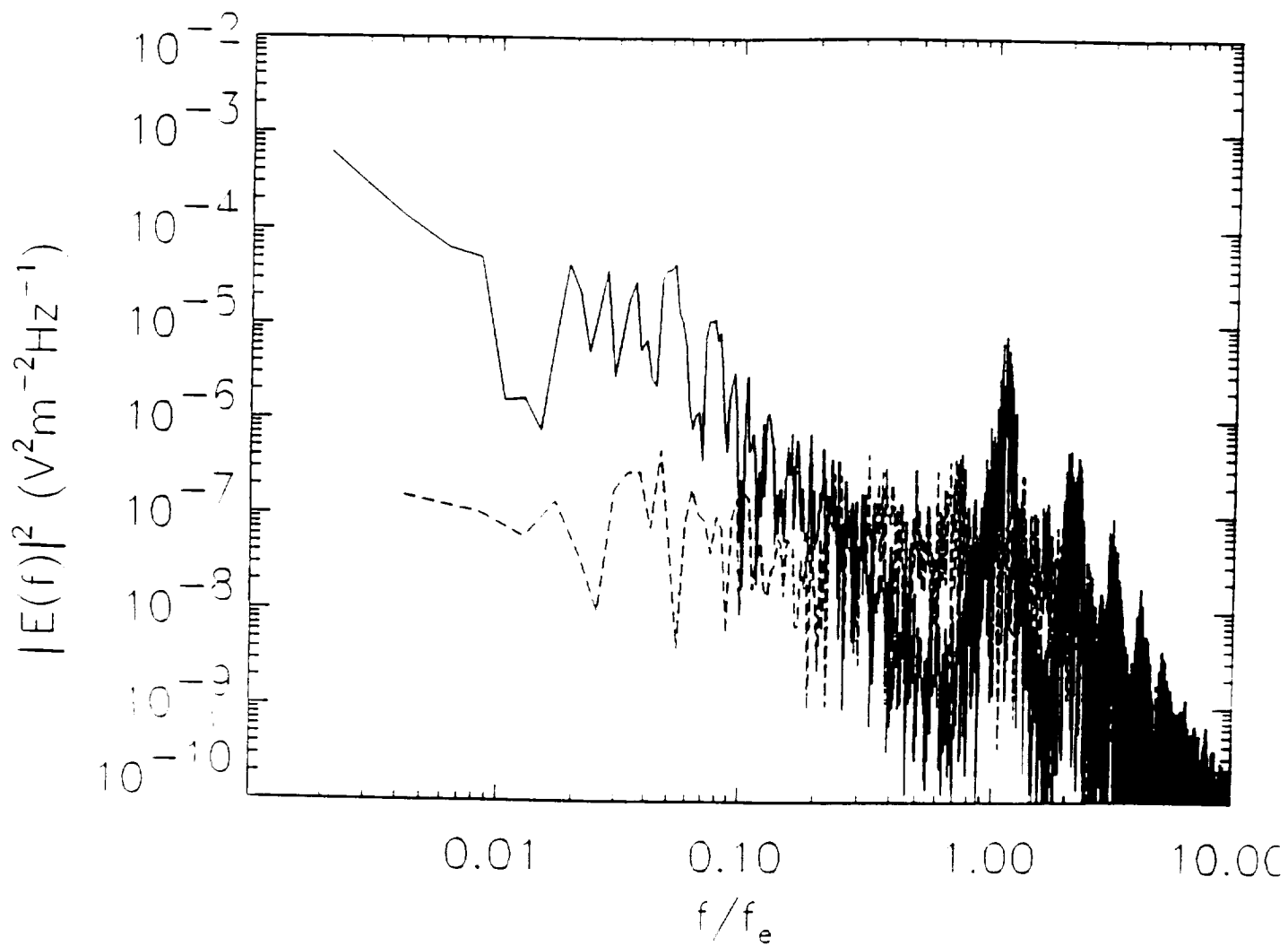
Figure 7. The frequency spectrum of the electrical field $E = (E_x^2 + E_y^2)^{1/2}$ is shown by the solid line. The electric field data for E_x and E_y are the same as plotted in Figures 6b and 6c. The broken line shows the frequency spectrum with zero drift for the water ions.
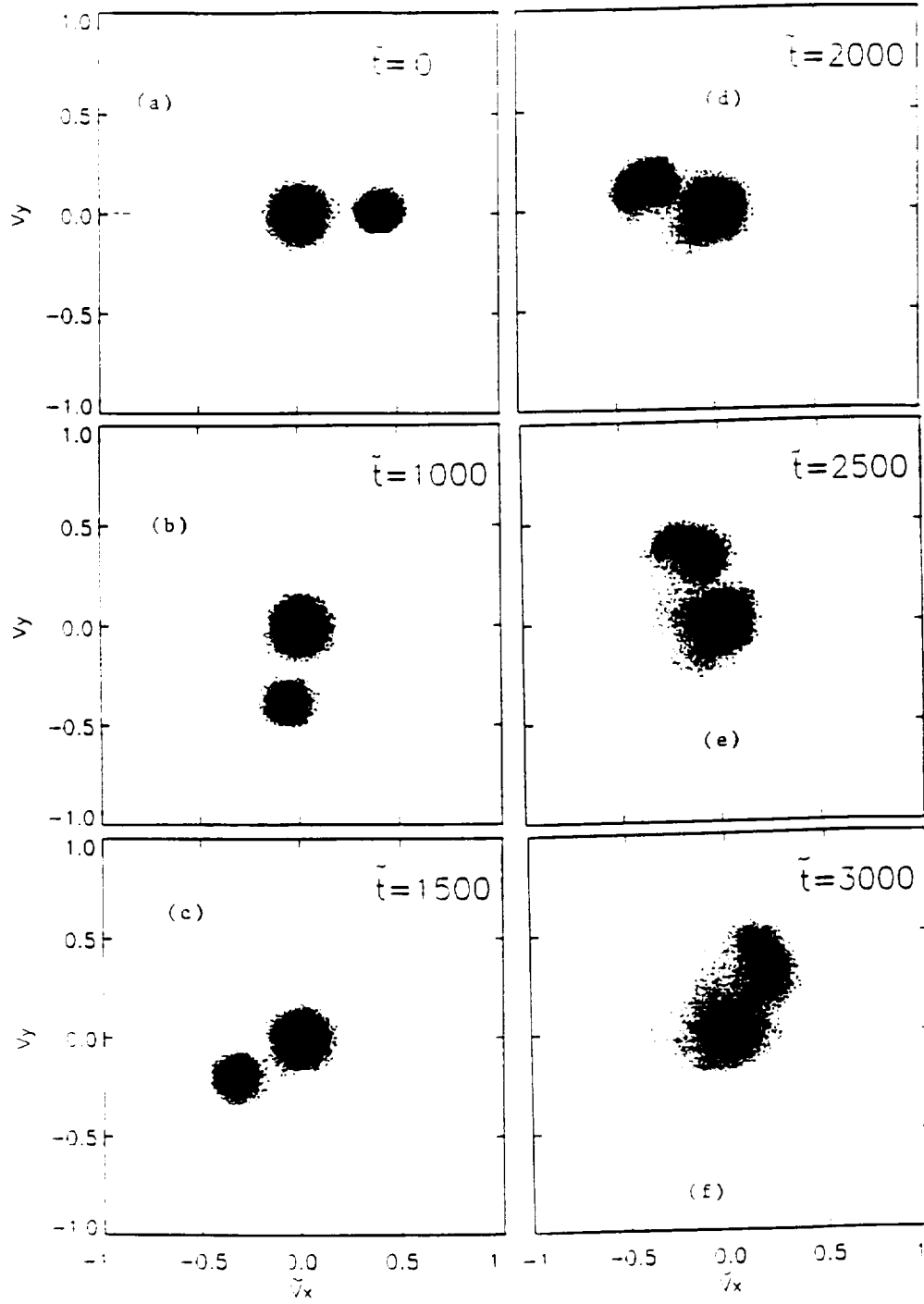
Figure 8. The gyration of water ions in the $V_x - V_y$ plane is shown for $\omega_e = \Omega_e$. Eventually the water and oxygen ions mix the velocity space as seen for $\bar{t} \geq 2000$.
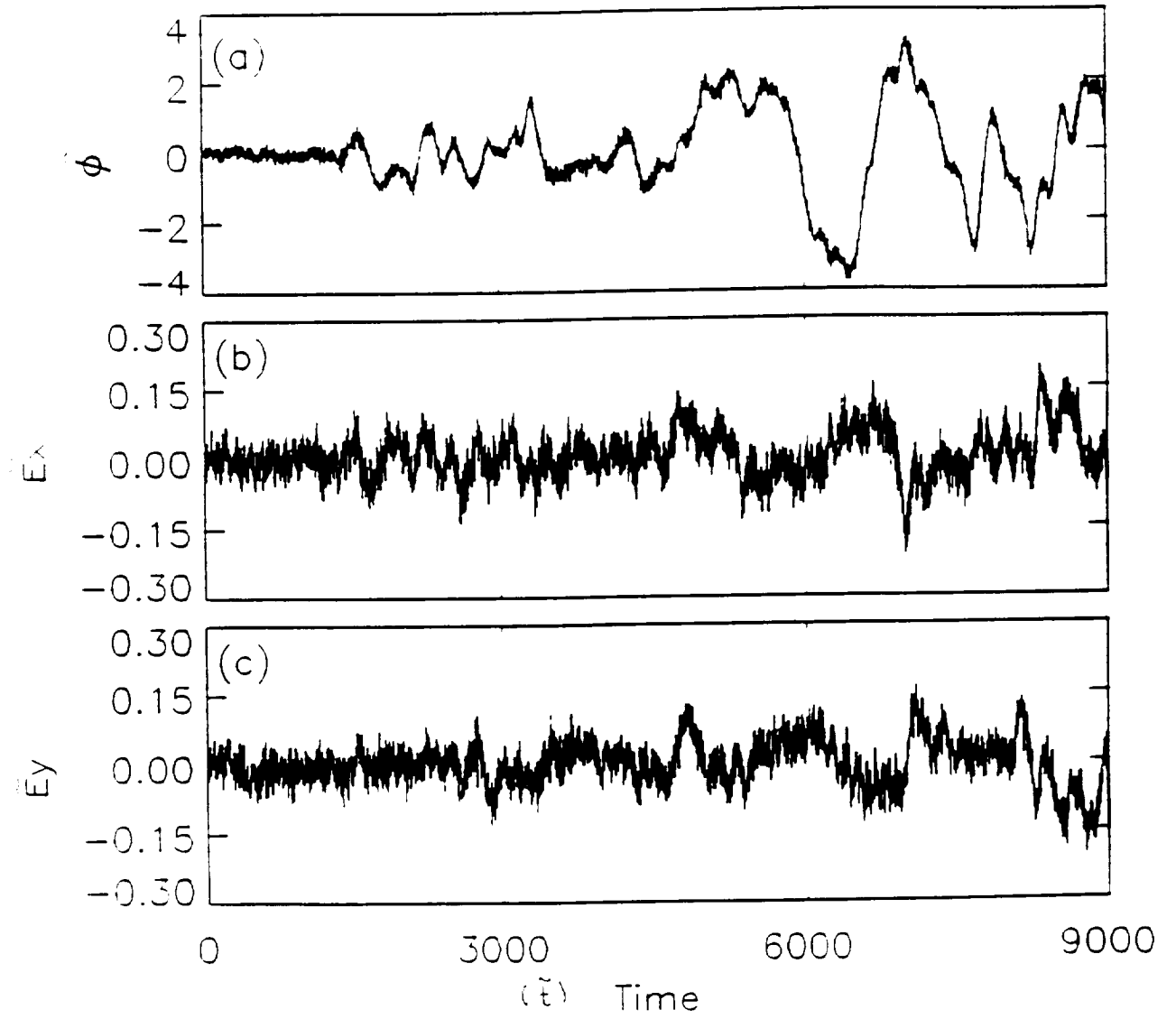
Figure 9. The same as Figure 6, but for $\Omega_e = 0.3\,\omega_e$, $n_w = 0.5\,N_o$, $m_o/m_e = 2048$, and $U = 0.2V_e$.
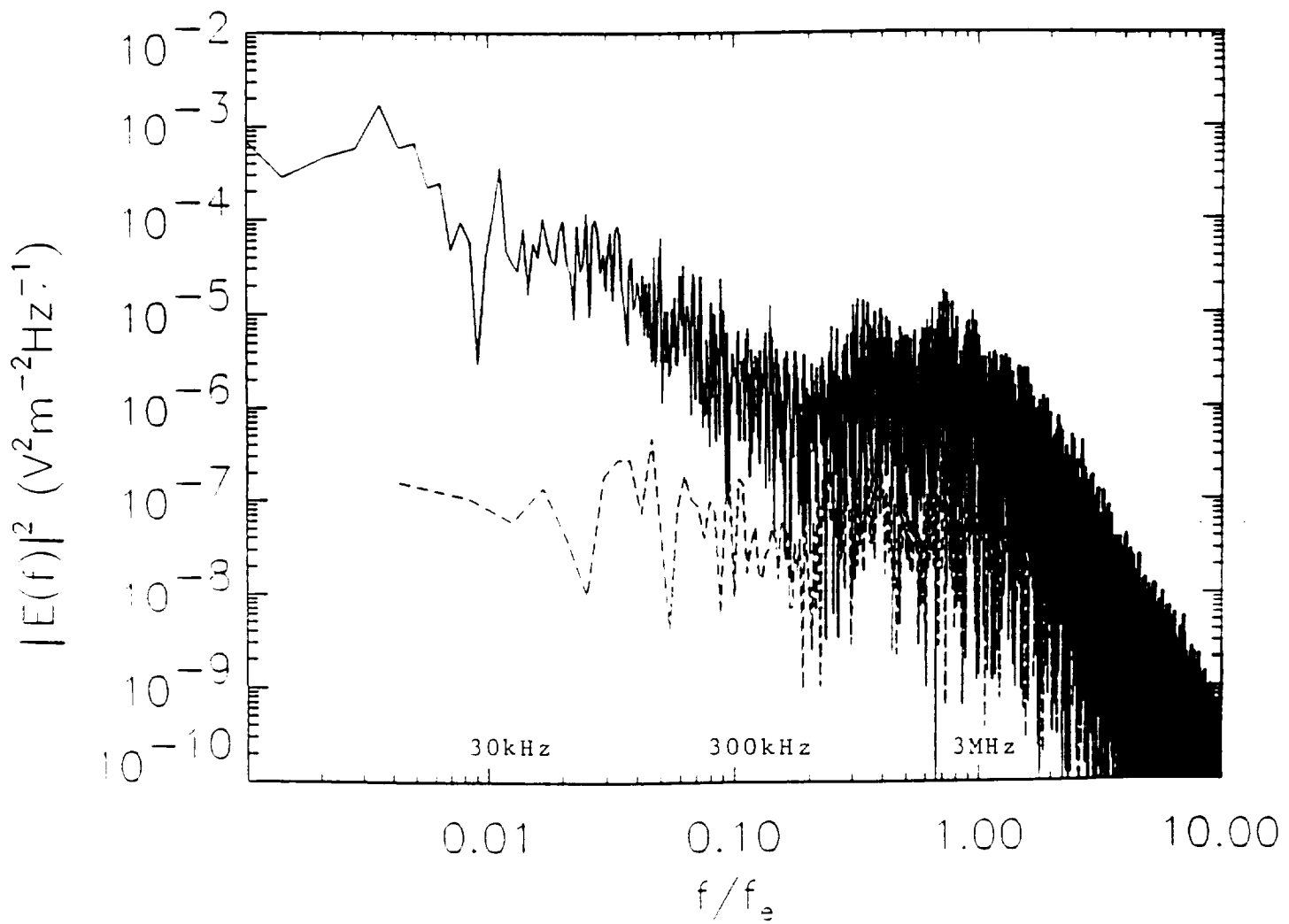
Figure 10. The same as Figure 7, but for $\Omega_e = 0.3\,\omega_e$, $n_w = 0.5\,N_o$, $m_o/m_e = 2048$, and $U = 0.2V_e$. The frequencies shown on the horizontal axis are for a plasma density $N_o = 10^5$ cm^{-3}.
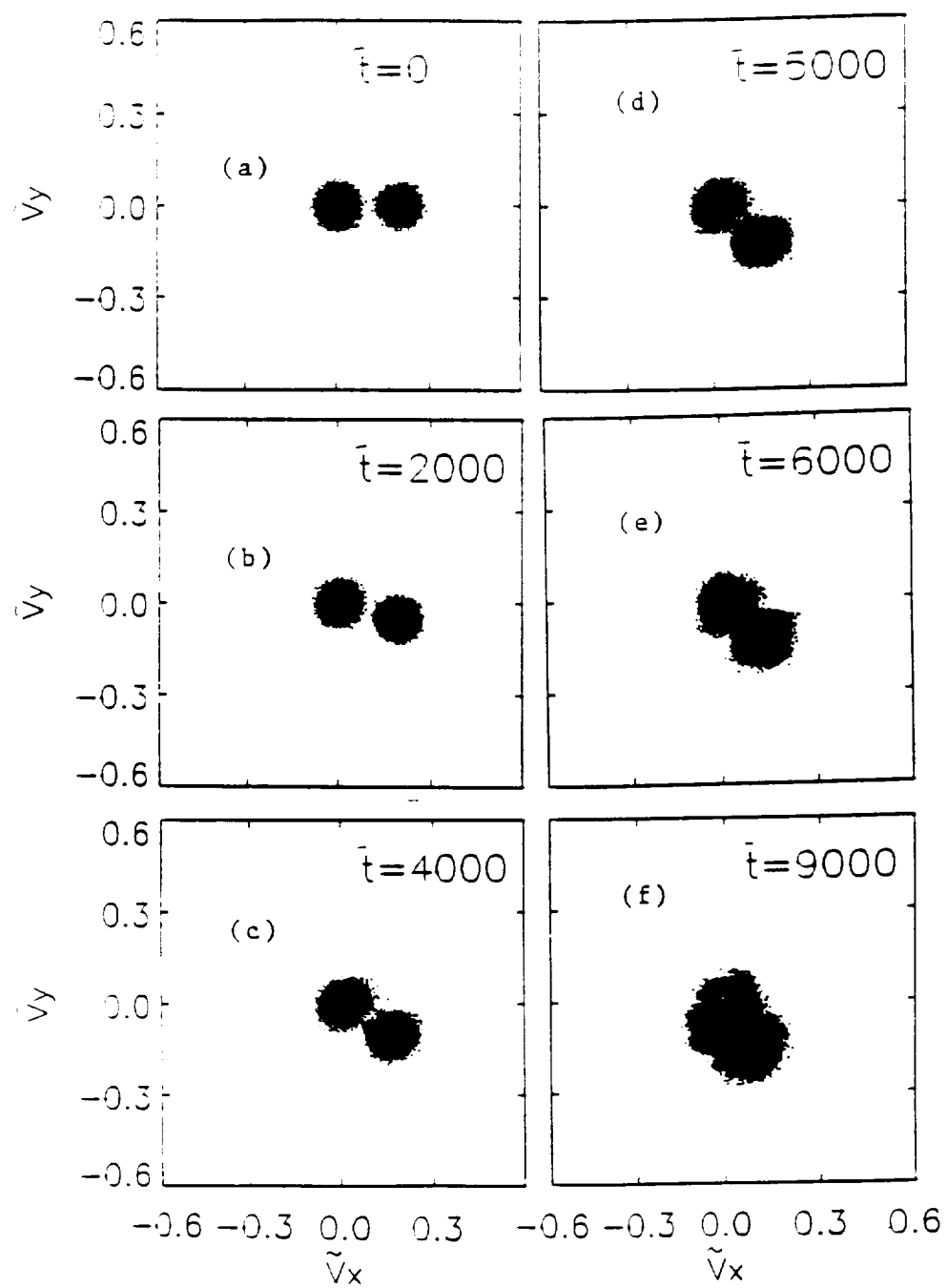
Figure 11. The same as Figure 8, but for $\Omega_e = 0.3\,\omega_e$, $m_o/m_e = 2048$, and $U = 0.2V_e'$.
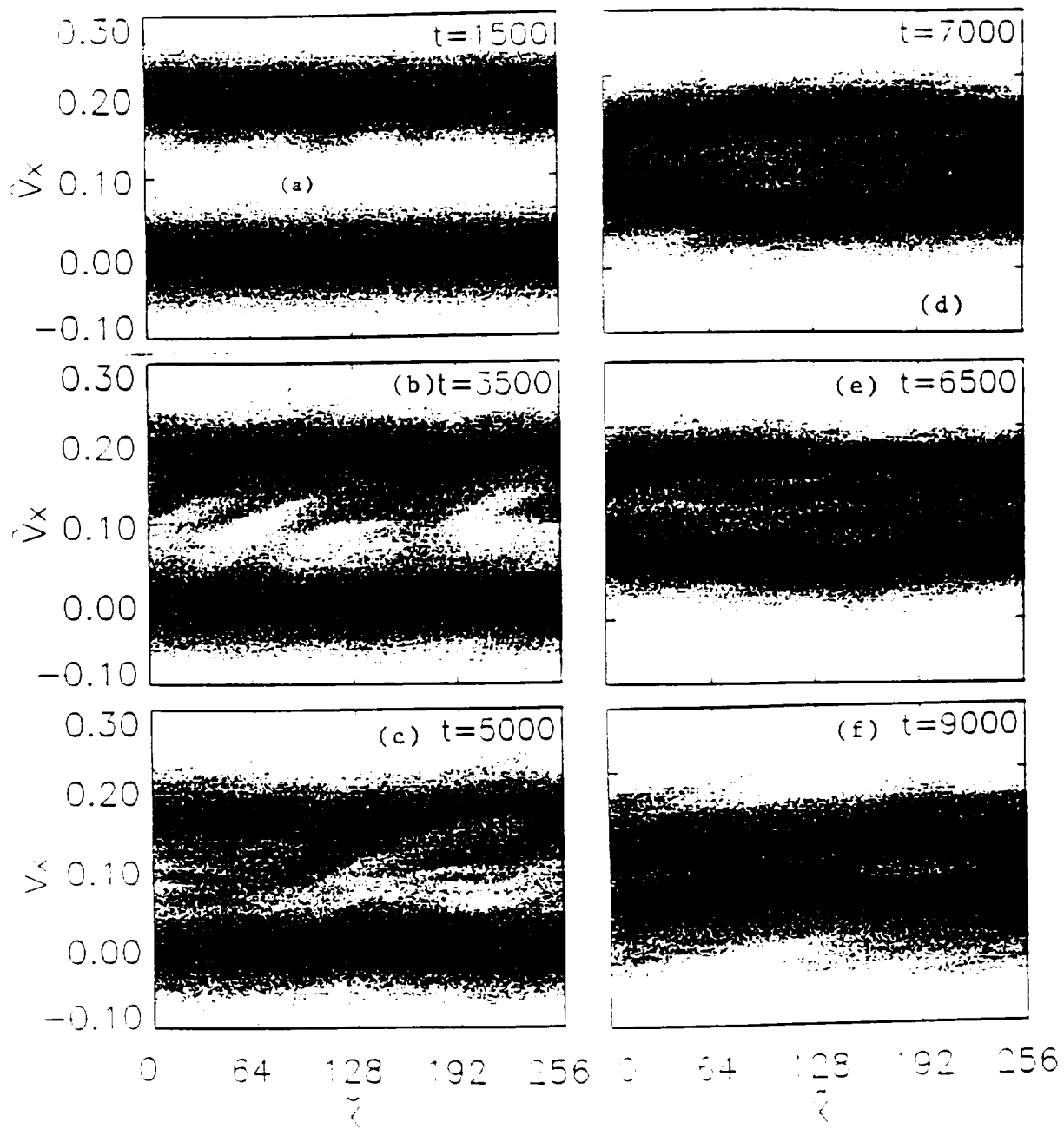
Figure 12. Ion phase space in the $X - V_x$ plane for the simulation results shown in Figures 9-11.
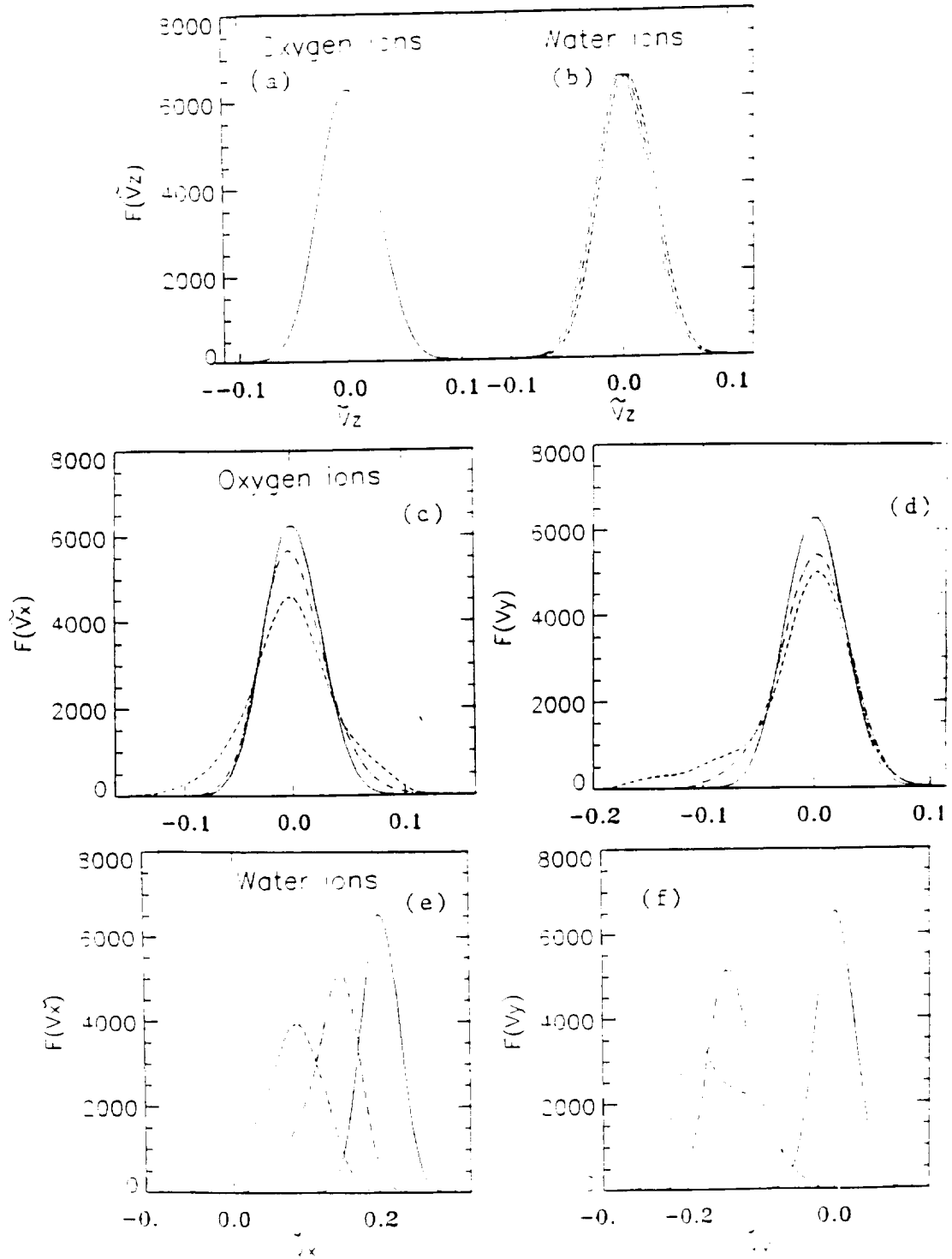
Figure 13. Ion velocity distribution functions from the simulation with $\Omega_e = 0.3\,\omega_e$, $n_w / N_o = 0.5$, $m_o / m_e = 2048$, and $U = 0.2V_e$. **(a)** $F(V_z)$ for O^+, **(b)** $F(V_z)$ for H_2O^+, **(c)** $F(V_x)$ for O^+, **(d)** $F(V_y)$ for O^+, **(e)** $F(V_x)$ for H_2O^+, and **(f)** $F(V_y)$ for H_2O^+. The solid curves are for $\bar{t} = 0$, dash-dot curves for $\bar{t} = 6000$, and the dashed curves for $\bar{t} = 9000$.
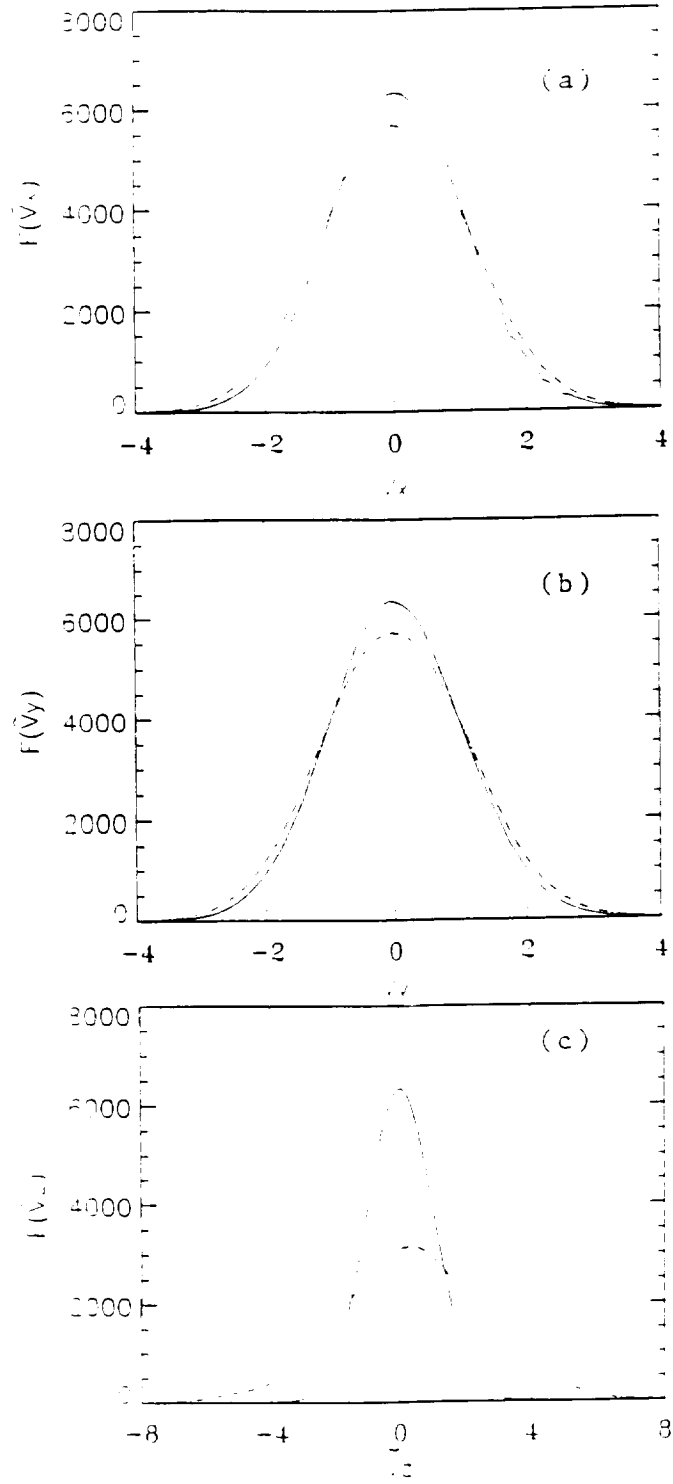
Figure 14. Electron distribution functions from the run with $\Omega_e = 0.3\,\omega_e$, $n_w / N_o = 0.5$, $m_o / m_e = 2048$, and $U = 0.2V_e$. (a) $F(V_x)$, (b) $F(V_y)$ and (c) $F(V_z)$. The solid curves are for $\bar{t} = 0$ and the dash-dot curves for $\bar{t} = 9000$.
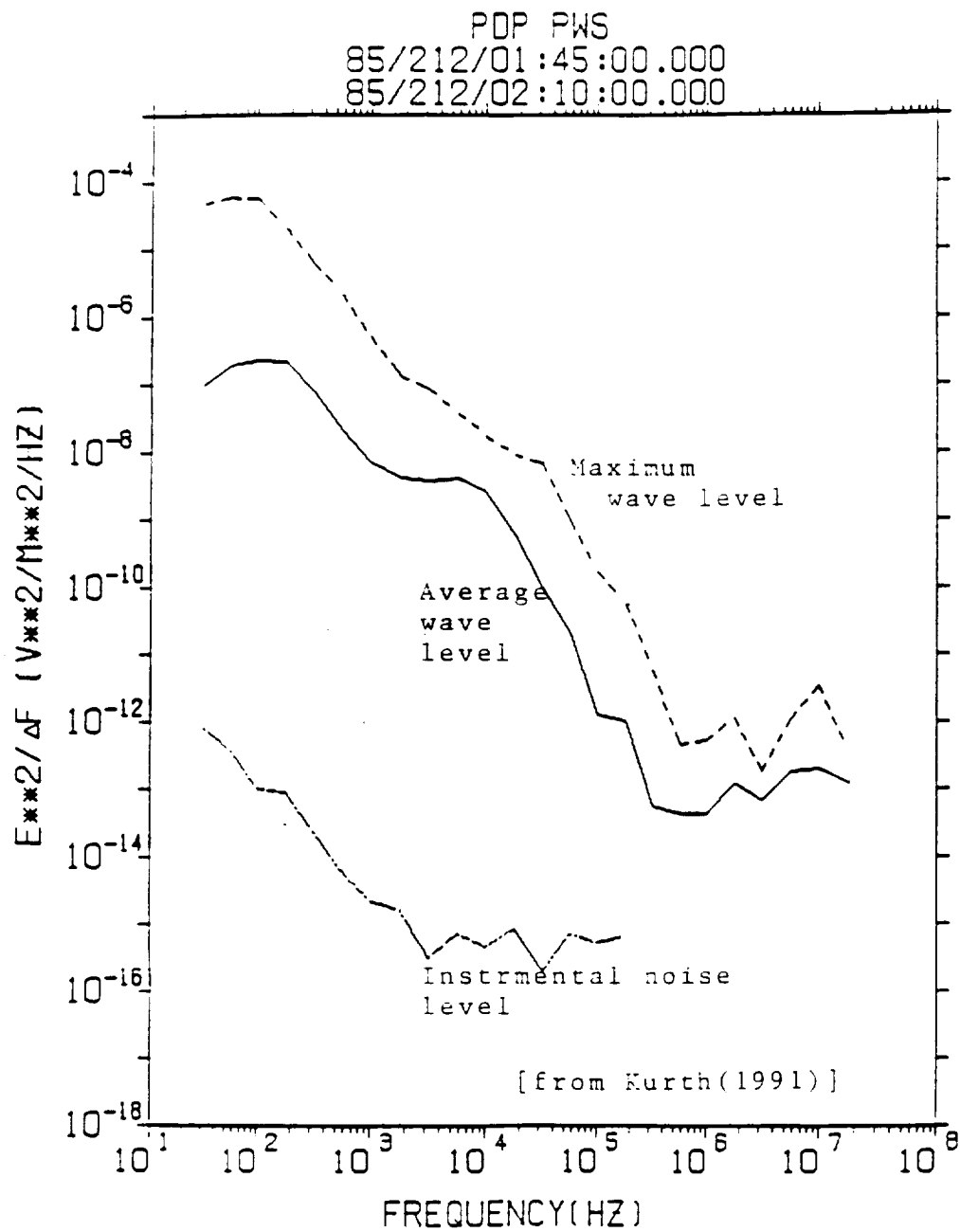
Figure 15. Typical frequency spectra of the electrostatic broadband noise measured from the space shuttle [Kurth, 1991; Cairns and Gurnett, 1992].

2.5 Dimensional Particle-In-Cell Code For Studying Wave Generation by Contaminant Ions Near a large spacecraft.

W.C. Leung and N. Singh

Department of Electrical and Computer Engineering,
University of Alabama, Huntsville.
Al 35899.

```
C**********************************************************************
C*          2.5 Dimensional Particle-In-Cell Code For Studing Wave Generation*
C*          by Contaminant Ions Near a large spacecraft.                *
C*                                                                      *
C*          Theta = 0.05 (Angle of the Magnetic field to the X-axis)    *
C*          Bm = 0.3 (Normalized Magnetic field)                        *
C*          Bxm = Bm*Sin(theta)                                         *
C*          Bym = 0                                                     *
C*          Bzm = Bm*Cos(theta)                                         *
C*          dx = 2 (Delta x)                                            *
C*          dy = 2 (Delta y)                                            *
C*          Time = Normalized time                                      *
C*          dt = 0.2 (Delta Time)                                       *
C*          Mass ratio of Oxygen Ions = 2048                            *
C*          Mass ratio of Water Ions = 2304                             *
C*          Only Water Ions have drift velocity of 0.2                  *
C*          Number of grid in x-direction = 128                         *
C*          Number of grid in y-direction = 64                          *
C**********************************************************************
        REAL ION
        COMMON/PAR/ELE(163840,5),ION(163840,5)
        COMMON/ARRAY1/PHI(129,65)
        COMMON/EFIELD/EX(129,65),EY(129,65)
        COMMON/ARRAY/RHO(129,65),RHOE(129,65),RHOI(129,65)
        COMMON/DEL/DVXI,VXIW(301),FIW(301),GIW(301),VDRI,DVXE,DVRE
     >             ,VXIO(301),FIO(301),GIO(301)
     >             ,VXEO(241),FEO(241),GEO(241)
        COMMON/VEX/XX(129),YY(65)
        COMMON TIME,NIJ
        COMMON NX,NY,NX1,NY1,PI,MAIN
        COMMON RATO,RATW,DELT,VELVAR,BXM,BYM,BZM,EYO
        COMMON ISEED,DY,DX,NIED,NIED1,NSUMO
C
        DELT=0.2
        TSTART = 0.
        TMAX = 9000.
        ITST = INT(TSTART)
        NIT = (TMAX-TSTART)/DELT + 1
        NX=129
        NY=65
        NX1=NX-1
        NY1=NY-1
        NIJ = 20
        ISEED=10000001
C
        CALL SET
        CALL DISTELE
        CALL DISTIONW
        CALL DISTIONO
        CALL BEGIN
        CALL INITIAL
C
        TIME=-0.2 + TSTART
        LWRTE = 1
        LAC = -1
C
        OPEN(UNIT=92,FILE='EXEY-MASSO10W10Fixd0.DAT',STATUS='NEW')
        OPEN(UNIT=93,FILE='PHI-MASSO10W10FIXD0.DAT',STATUS='NEW')
        OPEN(UNIT=94,FILE='RHO-MASSO10W10FIXD0.DAT',STATUS='NEW')
C
        DO 1 MAIN=0,NIT
           TIME=TIME+DELT
           LAC = LAC + 1
           CALL DENS
           CALL POTENT
           CALL FIELD
```

```
              CALL MOVEI
              CALL MOVEE
C
C        Write the Electric field, Potential and Charge Density at the
C        center point of the system at instance time.
C
              WRITE(92,41)TIME,EX(65,33),EY(65,33)
              WRITE(93,42)TIME,PHI(65,33)
              WRITE(94,42)TIME,RHO(65,33)
41            format(1x,f8.3,2e12.3)
42            format(1x,f8.3,e12.3)
C
C
              IF(LAC .EQ. 2500)THEN
                  ITIM = ITST + (LAC*LWRTE)/5
                  CALL WRITEFIL(ITIM)
                  LWRTE = LWRTE+1
                  LAC = 0
              ENDIF
C
1             CONTINUE
C
              CLOSE(92)
              CLOSE(93)
              CLOSE(94)
              STOP
              END

C*****************************************************************************
         SUBROUTINE INITIAL
C*****************************************************************************
         REAL ION
         COMMON/PAR/ELE(163840,5),ION(163840,5)
         COMMON/ARRAY1/PHI(129,65)
         COMMON/EFIELD/EX(129,65),EY(129,65)
         COMMON/ARRAY/RHO(129,65),RHOE(129,65),RHOI(129,65)
         COMMON/DEL/DVXI,VXIW(301),FIW(301),GIW(301),VDRI,DVXE,VDRE
     >              ,VXIO(301),FIO(301),GIO(301)
     >              ,VXEO(241),FEO(241),GEO(241)
         COMMON/VEX/XX(129),YY(65)
         COMMON TIME,NIJ
         COMMON NX,NY,NX1,NY1,PI,MAIN
         COMMON RATO,RATW,DELT,VELVAR,BXM,BYM,BZM,EYO
         COMMON ISEED,DY,DX,NIED,NIED1,NSUMO
C
         OPEN(UNIT=85,FILE='e-v_t0.dat',STATUS='NEW')
         OPEN(UNIT=86,FILE='e-p_t0.dat',STATUS='NEW')
         OPEN(UNIT=95,FILE='i-v_t0.dat',STATUS='NEW')
         OPEN(UNIT=96,FILE='i-p_t0.dat',STATUS='NEW')
C
         DO 55 L=1,NIED
             WRITE(95,19)ION(L,3),ION(L,4),ION(L,5)
19           FORMAT(1X,3E12.3)
55       .CONTINUE
C
         DO 56 L=1,NIED
             WRITE(96,17)ION(L,1),ION(L,2)
17           FORMAT(1X,2F9.3)
56       CONTINUE
C
         DO 57 L=1,NIED
             WRITE(86,17)ELE(L,1),ELE(L,2)
57       CONTINUE
C
         DO 58 L=1,NIED
             WRITE(85,19)ELE(L,3),ELE(L,4),ELE(L,5)
```

```
58       CONTINUE
C

         CLOSE(95)
         CLOSE(96)
         CLOSE(85)
         CLOSE(86)
         RETURN
         END


C  ****************************************************************
         SUBROUTINE WRITEFIL(ITIM)
C  ****************************************************************
C  ****************************************************************
      CHARACTER*15 NAME2,NAME3,NAME4,NAME5,NAME6,NAME7,
     >             NAME8,NAME9,NAME10,NAME11
      REAL ION
      COMMON/PAR/ELE(163840,5),ION(163840,5)
      COMMON/ARRAY1/PHI(129,65)
      COMMON/EFIELD/EX(129,65),EY(129,65)
      COMMON/ARRAY/RHO(129,65),RHOE(129,65),RHOI(129,65)
      COMMON/DEL/DVXI,VXIW(301),FIW(301),GIW(301),VDRI,DVXE,VDRE
     >          ,VXIO(301),FIO(301),GIO(301)
     >          ,VXEO(241),FEO(241),GEO(241)
      COMMON/VEX/XX(129),YY(65)
      COMMON TIME,NIJ
      COMMON NX,NY,NX1,NY1,PI,MAIN
      COMMON RATO,RATW,DELT,VELVAR,BXM,BYM,BZM,EYO
      COMMON ISEED,DY,DX,NIED,NIED1,NSUMO
C
      WRITE(NAME2,'(''phi_t'',i4)') ITIM
      OPEN(UNIT=2,FILE=NAME2,STATUS='NEW')
C
      WRITE(NAME3,'(''rhoi_t'',i4)') ITIM
      OPEN(UNIT=3,FILE=NAME3,STATUS='NEW')
C
      WRITE(NAME4,'(''rhoe_t'',i4)') ITIM
      OPEN(UNIT=4,FILE=NAME4,STATUS='NEW')
C
      WRITE(NAME5,'(''rho_t'',i4)') ITIM
      OPEN(UNIT=5,FILE=NAME5,STATUS='NEW')
C
      WRITE(NAME6,'(''ex_t'',i4)') ITIM
      OPEN(UNIT=6,FILE=NAME6,STATUS='NEW')
C
      WRITE(NAME7,'(''ey_t'',i4)') ITIM
      OPEN(UNIT=7,FILE=NAME7,STATUS='NEW')
C
      WRITE(NAME8,'(''e-p_t'',i4)') ITIM
      OPEN(UNIT=8,FILE=NAME8,STATUS='NEW')
C
      WRITE(NAME9,'(''e-v_t'',i4)') ITIM
      OPEN(UNIT=9,FILE=NAME9,STATUS='NEW')
C
      WRITE(NAME10,'(''i-p_t'',i4)') ITIM
      OPEN(UNIT=10,FILE=NAME10,STATUS='NEW')
C
      WRITE(NAME11,'(''i-v_t'',i4)') ITIM
      OPEN(UNIT=11,FILE=NAME11,STATUS='NEW')
C
      WRITE(NAME2,'(''phi_t'',i4)') ITIM
      OPEN(UNIT=2,FILE=NAME2,STATUS='NEW')
C
      DO 10 J=1,NY
        WRITE(2,112)(PHI(I,J),  I=1,NX)
        WRITE(3,112)(RHOI(I,J), I=1,NX)
        WRITE(4,112)(RHOE(I,J), I=1,NX)
```

```fortran
                WRITE(5,112)(RHO(I,J), I=1,NX)
                WRITE(6,112)(EX(I,J), I=1,NX)
                WRITE(7,112)(EY(I,J), I=1,NX)
112              FORMAT(1X,6E12.3)
10           CONTINUE
            CLOSE(2)
            CLOSE(3)
            CLOSE(4)
            CLOSE(5)
            CLOSE(6)
            CLOSE(7)
C
            DO 20 L=1,NIED
              WRITE(8,113)ELE(L,1),ELE(L,2)
20          CONTINUE
C
            DO 25 L=1,NIED
              WRITE(10,118)ION(L,1),ION(L,2)
118           format(1x,2f9.3)
25          CONTINUE
C
            DO 30 L=1,NIED
              WRITE(9,114)ELE(L,3),ELE(L,4),ELE(L,5)
30          CONTINUE
C
            DO 35 L=1,NIED
              WRITE(11,114)ION(L,3),ION(L,4),ION(L,5)
35          CONTINUE
C
113         FORMAT(1X,2F9.3)
114         FORMAT(1X,3E12.3)
C
            CLOSE(8)
            CLOSE(9)
            CLOSE(10)
            CLOSE(11)
C
            RETURN
            END


C     *****************************************************************
            SUBROUTINE SET
C     *****************************************************************
      REAL ION
      COMMON/PAR/ELE(163840,5),ION(163840,5)
      COMMON/ARRAY1/PHI(129,65)
      COMMON/EFIELD/EX(129,65),EY(129,65)
      COMMON/ARRAY/RHO(129,65),RHOE(129,65),RHOI(129,65)
      COMMON/DEL/DVXI,VXIW(301),FIW(301),GIW(301),VDRI,DVXE,VDRE
     >          ,VXIO(301),FIO(301),GIO(301)
     >          ,VXEO(241),FEO(241),GEO(241)
      COMMON/VEX/XX(129),YY(65)
      COMMON TIME,NIJ
      COMMON NX,NY,NX1,NY1,PI,MAIN
      COMMON RATO,RATW,DELT,VELVAR,BXM,BYM,BZM,EYO
      COMMON ISEED,DY,DX,NIED,NIED1,NSUMO
      COMMON COKX(129),COKY(65),SM(129,65)
C
      PI=3.1415926535898
C     Normalized Magnetic field
      BM=0.3
C     Angle of the magnetic field to the x-axis
      THETA=0.05
C     Magnetic field in Z-component
      BZM=BM*COS(THETA)
```

```fortran
C         Magentic field in Y-component
          BYM=0.
C         Magnetic field in X-component
          BXM=BM*SIN(THETA)
C         Normalized Water Ions Drift velocity
          VELVAR = 0.2
          EYO = 0.
          DX = 2.
          DY = 2.
          RATW = 1.0/(2304.)
          RATO = 1.0/(2048.)
C
          DO 1 J=1,NY
             YY(J)=DY*FLOAT(J-1)
    1     CONTINUE
          DO 2 I=1,NX
             XX(I)=DX*FLOAT(I-1)
    2     CONTINUE
C
       DO 10 I=1,NX1
         COKX(I) = ( 2.*PI*I/XX(NX) )**2
   10    CONTINUE
C
       DO 20 I=1,NY1
         COKY(I) = ( 2.*PI*I/YY(NY) )**2
   20    CONTINUE
C
C      Smoothing Coefficient
C
       DO 30 J=1,NY1
        DO 30 I=1,NX1
        SM(I,J) = (NX1*SIN(PI*I/NX1)*NY1*SIN(PI*J/NY1)/(PI*I*PI*J))**2
   30   CONTINUE
          RETURN
          END
C
C     ****************************************************************
          SUBROUTINE DISTIONW
C     ****************************************************************
       REAL ION
       COMMON/PAR/ELE(163840,5),ION(163840,5)
       COMMON/ARRAY1/PHI(129,65)
       COMMON/EFIELD/EX(129,65),EY(129,65)
       COMMON/ARRAY/RHO(129,65),RHOE(129,65),RHOI(129,65)
       COMMON/DEL/DVXI,VXIW(301),FIW(301),GIW(301),VDRI,DVXE,VDRE
      >          ,VXIO(301),FIO(301),GIO(301)
      >          ,VXEO(241),FEO(241),GEO(241)
       COMMON/VEX/XX(129),YY(65)
       COMMON TIME,NIJ
       COMMON NX,NY,NX1,NY1,PI,MAIN
       COMMON RATO,RATW,DELT,VELVAR,BXM,BYM,BZM,EYO
       COMMON ISEED,DY,DX,NIED,NIED1,NSUMO
C
       DVXI=0.00104
       VDRI = VELVAR
       VXIW(1) = 0.
       FIW(1) = 0.
       GIW(1) = 0.
       DO 10 I = 2,301
          VXIW(I) = FLOAT(I-1)*DVXI + VXIW(1)
          GIW(I) =EXP(-(576.*4.*(VXIW(I)-VDRI)**2)/2)
          FIW(I) = DVXI*0.5*(GIW(I-1)+GIW(I))+FIW(I-1)
   10  CONTINUE
C
       DO 20 J = 1,301
          FIW(J) = FIW(J)/FIW(301)
```

```
   20     CONTINUE
          RETURN
          END
   C
   C
   C     ************************************************************
          SUBROUTINE DISTELE
   C     ************************************************************C
          REAL ION
          COMMON/PAR/ELE(163840,5),ION(163840,5)
          COMMON/ARRAY1/PHI(129,65)
          COMMON/EFIELD/EX(129,65),EY(129,65)
          COMMON/ARRAY/RHO(129,65),RHOE(129,65),RHOI(129,65)
          COMMON/DEL/DVXI,VXIW(301),FIW(301),GIW(301),VDRI,DVXE,VDRE
         >          ,VXIO(301),FIO(301),GIO(301)
         >          ,VXEO(241),FEO(241),GEO(241)
          COMMON/VEX/XX(129),YY(65)
          COMMON TIME,NIJ
          COMMON NX,NY,NX1,NY1,PI,MAIN
          COMMON RATO,RATW,DELT,VELVAR,BXM,BYM,BZM,EYO
          COMMON ISEED,DY,DX,NIED,NIED1,NSUMO
   C
          DVXE=0.05
          VDRE = 0.
          VXEO(1) = -6.
          FEO(1) = 0.
          GEO(1) = 0.
          DO 10 I = 2,241
              VXEO(I) = FLOAT(I-1)*DVXE + VXEO(1)
              GEO(I) =EXP(-((VXEO(I)-VDRE)**2)/2)
              FEO(I) = DVXE*0.5*(GEO(I-1)+GEO(I))+FEO(I-1)
   10     CONTINUE
   C
          DO 20 J = 1,241
              FEO(J) = FEO(J)/FEO(241)
   20     CONTINUE
          RETURN
          END


   C     ************************************************************
          SUBROUTINE DISTIONO
   C     ************************************************************
          REAL ION
          COMMON/PAR/ELE(163840,5),ION(163840,5)
          COMMON/ARRAY1/PHI(129,65)
          COMMON/EFIELD/EX(129,65),EY(129,65)
          COMMON/ARRAY/RHO(129,65),RHOE(129,65),RHOI(129,65)
          COMMON/DEL/DVXI,VXIW(301),FIW(301),GIW(301),VDRI,DVXE,VDRE
         >          ,VXIO(301),FIO(301),GIO(301)
         >          ,VXEO(241),FEO(241),GEO(241)
          COMMON/VEX/XX(129),YY(65)
          COMMON TIME,NIJ
          COMMON NX,NY,NX1,NY1,PI,MAIN
          COMMON RATO,RATW,DELT,VELVAR,BXM,BYM,BZM,EYO
          COMMON ISEED,DY,DX,NIED,NIED1,NSUMO
   C
          DVXI=0.0011
          VDRI = 0.
          VXIO(1) = -0.1325
          FIO(1) = 0.
          GIO(1) = 0.
          DO 10 I = 2,301
              VXIO(I) = FLOAT(I-1)*DVXI + VXIO(1)
   C          VXIO(I) = FLOAT(I-1)*DVXI
              GIO(I) =EXP(-(512.*4.*(VXIO(I)-VDRI)**2)/2)
              FIO(I) = DVXI*0.5*(GIO(I-1)+GIO(I))+FIO(I-1)
   10     CONTINUE
```

```fortran
CC
           DO 20 J = 1,301
               FIO(J) = FIO(J)/FIO(301)
    20     CONTINUE
           RETURN
           END

C     ************************************************************
           SUBROUTINE BEGIN
C     ************************************************************
           REAL ION
           COMMON/PAR/ELE(163840,5),ION(163840,5)
           COMMON/ARRAY1/PHI(129,65)
           COMMON/EFIELD/EX(129,65),EY(129,65)
           COMMON/ARRAY/RHO(129,65),RHOE(129,65),RHOI(129,65)
           COMMON/DEL/DVXI,VXIW(301),FIW(301),GIW(301),VDRI,DVXE,VDRE
      >              ,VXIO(301),FIO(301),GIO(301)
      >              ,VXEO(241),FEO(241),GEO(241)
           COMMON/VEX/XX(129),YY(65)
           COMMON TIME,NIJ
           COMMON NX,NY,NX1,NY1,PI,MAIN
           COMMON RATO,RATW,DELT,VELVAR,BXM,BYM,BZM,EYO
           COMMON ISEED,DY,DX,NIED,NIED1,NSUMO

           PI= 3.1415926535898
           TPI = 2.*PI
C
C
C        Distribute 20 electrons per cell in the system
C
           NSUM = -3
           DO 13 J=1,NY1
            DO 14 I=1,NX1
               DO 12 M=1,3
                 NSUM = NSUM + 3
                 DO 11 L=1,3
                    ELE(L+NSUM,1)= 0.5*L + DX*(I-1)
                    ELE(L+NSUM,2)= 0.5*M + DY*(J-1)
                 RND = RAN(ISEED)
                 DO 40 K=1,241
                 DIFF1=FEO(K)-RND
                 IF(DIFF1 .GE. 0.0) GOTO 20
    40           CONTINUE
    20           ELE(L+NSUM,3) = VXEO(K)
                 VPAR = 1.414*SQRT(-LOG(1-RAN(ISEED)))
                 TPAR = TPI*RAN(ISEED)
                 ELE(L+NSUM,4) = VPAR*SIN(TPAR)
                 ELE(L+NSUM,5) = VPAR*COS(TPAR)
    11           CONTINUE
    12         CONTINUE
    14       CONTINUE
    13     CONTINUE
c
           DO 133 J=1,NY1
            DO 144 I=1,NX1
               DO 122 M=1,3
                 NSUM = NSUM + 3
                 DO 111 L=1,3
                    ELE(L+NSUM,1)= 0.5*L + DX*(I-1) + 0.25
                    ELE(L+NSUM,2)= 0.5*M + DY*(J-1) - 0.25
                 RND = RAN(ISEED)
                 DO 440 K=1,241
                 DIFF1=FEO(K)-RND
                 IF(DIFF1 .GE. 0.0) GOTO 220
    440          CONTINUE
    220          ELE(L+NSUM,3) = VXEO(K)
                 VPAR = 1.414*SQRT(-LOG(1-RAN(ISEED)))
```

```
                  TPAR = TPI*RAN(ISEED)
                  ELE(L+NSUM,4) = VPAR*SIN(TPAR)
                  ELE(L+NSUM,5) = VPAR*COS(TPAR)
  111              CONTINUE
  122             CONTINUE
  144           CONTINUE
  133           CONTINUE
    c

           NSUM = NSUM+3
           DO 83 J=1,NY1
            DO 84 I=1,NX1
              DO 82 M=1,3
                DO 81 L=1,3
                  IF(((L .EQ. 1).AND.(M .EQ. 1))
       >            .OR. ((L .EQ. 3).AND.(M .EQ. 3)))THEN
                  NSUM = NSUM + 1
                  ELE(NSUM,1)= 0.5*L + DX*(I-1) - 0.25
                  ELE(NSUM,2)= 0.5*M + DY*(J-1) + 0.25
              RND = RAN(ISEED)
              DO 484 K=1,241
              DIFF1=FEO(K)-RND
              IF(DIFF1 .GE. 0.0) GOTO 282
  484          CONTINUE
  282          ELE(NSUM,3) = VXEO(K)
               VPAR = 1.414*SQRT(-LOG(1-RAN(ISEED)))
               TPAR = TPI*RAN(ISEED)
               ELE(NSUM,4) = VPAR*SIN(TPAR)
               ELE(NSUM,5) = VPAR*COS(TPAR)
             ENDIF
  81           CONTINUE
  82          CONTINUE
  84         CONTINUE
  83         CONTINUE
    C

         PRINT*,'Total Number of Electrons in the system =',NSUM
    C
    C    Distribute 10 Oxygen Ions per cell in the sysytem
    C
         NSUMO = 0
         DO 313 J=1,NY1
          DO 314 I=1,NX1
             DO 312 M=1,3
               DO 511 L=1,3
                 NSUMO = NSUMO + 1
                 ION(NSUMO,1)= 0.5*L + DX*(I-1) + 0.25
                 ION(NSUMO,2)= 0.5*M + DY*(J-1) - 0.25
             RND = RAN(ISEED)
             DO 409 K=1,301
             DIFF1=FIO(K)-RND
             IF(DIFF1 .GE. 0.0) GOTO 209
  409         CONTINUE
  209         ION(NSUMO,3) = VXIO(K)
              VPAR = 0.03125*SQRT(-LOG(1-RAN(ISEED)))
              TPAR = TPI*RAN(ISEED)
              ION(NSUMO,4) = VPAR*SIN(TPAR)
              ION(NSUMO,5) = VPAR*COS(TPAR)
  511           CONTINUE
  312          CONTINUE
  314         CONTINUE
  313         CONTINUE
    C
         DO 73 J=1,NY1
          DO 74 I=1,NX1
             DO 72 M=1,3
               DO 71 L=1,3
                 IF((L .EQ. 1) .AND. (M .EQ. 1))THEN
```

```fortran
                            NSUMO = NSUMO + 1
                            ION(NSUMO,1)= 0.5*L + DX*(I-1) - 0.25
                            ION(NSUMO,2)= 0.5*M + DY*(J-1) + 0.25
C
                    RND = RAN(ISEED)
                    DO 479 K=1,301
                    DIFF1=FIO(K)-RND
                    IF(DIFF1 .GE. 0.0) GOTO 279
479                 CONTINUE
279                 ION(NSUMO,3) = VXIO(K)
C                   SQRT(100) =10.
C                   1/10. = 0.1
C                   1.414 * 0.1  = 0.1414
C                     VPAR = 0.0666667*SQRT(-LOG(1-RAN(ISEED)))
                    VPAR = 0.03125*SQRT(-LOG(1-RAN(ISEED)))
                    TPAR = TPI*RAN(ISEED)
                    ION(NSUMO,4) = VPAR*SIN(TPAR)
                    ION(NSUMO,5) = VPAR*COS(TPAR)
                    ENDIF
71                  CONTINUE
72                CONTINUE
74              CONTINUE
73              CONTINUE
C
        PRINT*,'Total Number of Oxygen Ions in the system=',NSUMO
C
C       Distribute 10 Water Ions per cell in the system
C
        NSUM = NSUMO
        DO 713 J=1,NY1
         DO 714 I=1,NX1
            DO 712 M=1,3
              DO 711 L=1,3
                NSUM = NSUM + 1
                ION(NSUM,1)= 0.5*L + DX*(I-1) - 0.125
                ION(NSUM,2)= 0.5*M + DY*(J-1) + 0.125
            RND = RAN(ISEED)
            DO 461 K=1,301
            DIFF1=FIW(K)-RND
            IF(DIFF1 .GE. 0.0) GOTO 261
461         CONTINUE
261         ION(NSUM,3) = VXIW(K)
            VPAR = 0.0295*SQRT(-LOG(1-RAN(ISEED)))
            TPAR = TPI*RAN(ISEED)
            ION(NSUM,4) = VPAR*SIN(TPAR)
            ION(NSUM,5) = VPAR*COS(TPAR)
711           CONTINUE
712           CONTINUE
714         CONTINUE
713         CONTINUE
C
        DO 613 J=1,NY1
         DO 614 I=1,NX1
            DO 612 M=1,3
              DO 611 L=1,3
                IF((L .EQ. 1).AND.(M .EQ. 1))THEN
                NSUM = NSUM + 1
                ION(NSUM,1)= 0.5*L + DX*(I-1) + 0.125
                ION(NSUM,2)= 0.5*M + DY*(J-1) - 0.125
            RND = RAN(ISEED)
            DO 661 K=1,301
            DIFF1=FIW(K)-RND
            IF(DIFF1 .GE. 0.0) GOTO 264
661         CONTINUE
264         ION(NSUM,3) = VXIW(K)
            VPAR = 0.0295*SQRT(-LOG(1-RAN(ISEED)))
```

```fortran
                 TPAR = TPI*RAN(ISEED)
                 ION(NSUM,4) = VPAR*SIN(TPAR)
                 ION(NSUM,5) = VPAR*COS(TPAR)
              ENDIF
611              CONTINUE
612             CONTINUE
614           CONTINUE
613           CONTINUE
C

          PRINT*,'Total Number of Ions in the system=',NSUM
          NIED = NSUM
          NIED1 = NIED -1
          RETURN
          END

C *****************************************************************
          SUBROUTINE DENS
C *****************************************************************
          INTEGER SIGR,SIGT
          REAL ION
          COMMON/PAR/ELE(163840,5),ION(163840,5)
          COMMON/ARRAY1/PHI(129,65)
          COMMON/EFIELD/EX(129,65),EY(129,65)
          COMMON/ARRAY/RHO(129,65),RHOE(129,65),RHOI(129,65)
          COMMON/DEL/DVXI,VXIW(301),FIW(301),GIW(301),VDRI,DVXE,DVRE
     >             ,VXIO(301),FIO(301),GIO(301)
     >             ,VXEO(241),FEO(241),GEO(241)
          COMMON/VEX/XX(129),YY(65)
          COMMON TIME,NIJ
          COMMON NX,NY,NX1,NY1,PI,MAIN
          COMMON RATO,RATW,DELT,VELVAR,BXM,BYM,BZM,EYO
          COMMON ISEED,DY,DX,NIED,NIED1,NSUMO
C
          DO 6 J=1,NY
             DO 5 I=1,NX
                RHOE(I,J)=0.
                RHOI(I,J)=0.
                RHO(I,J)=0.
5            CONTINUE
6         CONTINUE
C
          DO 1 L=1,NIED
             NII=INT(ELE(L,2)/DY)+1
C             IF(NII .EQ. NY+1)NII=1
             NJ=INT(ELE(L,1)/DX)+1
C
                 SIGR=+1
                 SIGT=+1
                 DELA=ABS(ELE(L,1)-XX(NJ))
                 DELB=ABS(ELE(L,2)-YY(NII))
                 A1=DELA*DELB
                 A2=DX*DELB-A1
                 A3=DY*DELA-A1
                 TOTA=DX*DY
                 A4=TOTA-(A1+A2+A3)
C

         RHOE(NJ+SIGR,NII+SIGT)=RHOE(NJ+SIGR,NII+SIGT)+A1/TOTA
         RHOE(NJ,NII+SIGT)=RHOE(NJ,NII+SIGT)+A2/TOTA
         RHOE(NJ+SIGR,NII)=RHOE(NJ+SIGR,NII)+A3/TOTA
         RHOE(NJ,NII)=RHOE(NJ,NII)+A4/TOTA
1        CONTINUE
C
         DO 2 L=1,NIED
             NII=INT(ION(L,2)/DY)+1
C             IF(NII .EQ. NY+1)NII=1
```

```
                NJ=INT(ION(L,1)/DX)+1
                    SIGR=+1
                    SIGT=+1
                   DELA=ABS(ION(L,1)-XX(NJ))
                   DELB=ABS(ION(L,2)-YY(NII))
                   A1=DELA*DELB
                   A2=DX*DELB-A1
                   A3=DY*DELA-A1
                   TOTA=DX*DY
                   A4=TOTA-(A1+A2+A3)
C
C

         RHOI(NJ+SIGR,NII+SIGT)=RHOI(NJ+SIGR,NII+SIGT)+A1/TOTA
         RHOI(NJ,NII+SIGT)=RHOI(NJ,NII+SIGT)+A2/TOTA
         RHOI(NJ+SIGR,NII)=RHOI(NJ+SIGR,NII)+A3/TOTA
         RHOI(NJ,NII)=RHOI(NJ,NII)+A4/TOTA
    2    CONTINUE
C
         DO 100 I=1,NX
         RHOI(I,1)=RHOI(I,1)+RHOI(I,NY)
         RHOI(I,NY)=RHOI(I,1)
         RHOE(I,1)=RHOE(I,1)+RHOE(I,NY)
         RHOE(I,NY)=RHOE(I,1)
  100    CONTINUE
C
         DO 108 J=1,NY
         RHOI(1,J)=RHOI(1,J)+RHOI(NX,J)
         RHOI(NX,J)=RHOI(1,J)
         RHOE(1,J)=RHOE(1,J)+RHOE(NX,J)
         RHOE(NX,J)=RHOE(1,J)
  108    CONTINUE
C
         DO 10 J=1,NY
            DO 11 I=1,NX
              RHOI(I,J) = RHOI(I,J)/NIJ
              RHOE(I,J) = RHOE(I,J)/NIJ
   11       CONTINUE
   10    CONTINUE
C
         DO 4 J=1,NY
           DO 8 I=1,NX
            RHO(I,J)= RHOI(I,J)-RHOE(I,J)
    8      CONTINUE
    4    CONTINUE
C
         RETURN
         END

C    ****************************************************************
         SUBROUTINE POTENT
C    ****************************************************************
         INTEGER NRA,NCA,LDA,LDCOEF
         COMPLEX RHOCOMP(129,65),PHICOMP(129,65)
         REAL ION
         COMMON/PAR/ELE(163840,5),ION(163840,5)
         COMMON/ARRAY1/PHI(129,65)
         COMMON/EFIELD/EX(129,65),EY(129,65)
         COMMON/ARRAY/RHO(129,65),RHOE(129,65),RHOI(129,65)
         COMMON/DEL/DVXI,VXIW(301),FIW(301),GIW(301),VDRI,DVXE,VDRE
     >            ,VXIO(301),FIO(301),GIO(301)
     >            ,VXEO(241),FEO(241),GEO(241)
         COMMON/VEX/XX(129),YY(65)
         COMMON TIME,NIJ
         COMMON NX,NY,NX1,NY1,PI,MAIN
         COMMON RATO,RATW,DELT,VELVAR,BXM,BYM,BZM,EYO
         COMMON ISEED,DY,DX,NIED,NIED1,NSUMO
```

```fortran
      COMMON COKX(129),COKY(65),SM(129,65)
      DIMENSION NN(2),DATA(16384)
C     DATA(2*NX1*NY1)
      PI = 3.1415926535898
      TPI = 2.*PI
      NN(1) = NX1
      NN(2) = NY1
C     SKIP I=1 (LENGHT=0) BECAUSE IT SHOULD START FROM LENGTH=1
      L= 2*NX1
      DO 10 J=2,NY
        DO 10 I=2,NX
          DATA( 2*(I-2) +1 + L * (J-2)   ) = RHO(I,J)
          DATA( 2*(I-1) + L * (J-2) ) = 0.
10    CONTINUE
C
C     Using two dimensioal FFT.(forward)
C      CALL FOURN(DATA,NN,NDIM,ISIGN)
      CALL FOURN(DATA,NN,2,1)
C
      DO 20 J=2,NY
        DO 20 I=2,NX
          REALRHOT =  DATA( 2*(I-2) +1 + L * (J-2)   )
          AIMAGRHOT=  DATA( 2*(I-1) + L * (J-2) )
          RHOCOMP(I,J) = REALRHOT*(1.,0.) + AIMAGRHOT*(0.,1.)
20    CONTINUE
C
      DO 30 J=2,NY
        DO 40 I=2,NX
          PHICOMP(I,J)=RHOCOMP(I,J)*SM(I-1,J-1)/(COKX(I-1)+COKY(J-1))
40      CONTINUE
30    CONTINUE
C
      DO 100 J=2,NY
        DO 100 I=2,NX
          DATA( 2*(I-2) +1 + L * (J-2)   ) = REAL(PHICOMP(I,J))
          DATA( 2*(I-1) + L * (J-2) ) = AIMAG(PHICOMP(I,J))
100   CONTINUE
C
C      Using two dimensional FFT.(backward)
C      CALL FOURN(DATA,NN,NDIM,ISIGN)
      CALL FOURN(DATA,NN,2,-1)
C
      DO 200 J=2,NY
        DO 200 I=2,NX
          REALPHIT =  DATA( 2*(I-2) +1 + L * (J-2)   )
          AIMAGPHIT=  DATA( 2*(I-1) + L * (J-2) )
          PHICOMP(I,J) = REALPHIT*(1.,0.) + AIMAGPHIT*(0.,1.)
200   CONTINUE
C
      DO 50 I=2,NX
        DO 60 J=2,NY
C         PHI(I,J) = REAL(PHICOMP(I,J))/(XX(NX) * YY(NY))
          PHI(I,J) = REAL(PHICOMP(I,J))/(NX1*NY1)
60      CONTINUE
50    CONTINUE
C
      DO 80 J=1,NY
          PHI(1,J) = PHI(NX,J)
80    CONTINUE
      DO 90 I=1,NX
          PHI(I,1) = PHI(I,NY)
90    CONTINUE
C
      RETURN
      END
C
```

```fortran
C     ***********************************************************
C           SUBROUTINE FIELD
C     ***********************************************************
      REAL ION
      COMMON/PAR/ELE(163840,5),ION(163840,5)
      COMMON/ARRAY1/PHI(129,65)
      COMMON/EFIELD/EX(129,65),EY(129,65)
      COMMON/ARRAY/RHO(129,65),RHOE(129,65),RHOI(129,65)
      COMMON/DEL/DVXI,VXIW(301),FIW(301),GIW(301),VDRI,DVXE,VDRE
     >          ,VXIO(301),FIO(301),GIO(301)
     >          ,VXEO(241),FEO(241),GEO(241)
      COMMON/VEX/XX(129),YY(65)
      COMMON TIME,NIJ
      COMMON NX,NY,NX1,NY1,PI,MAIN
      COMMON RATO,RATW,DELT,VELVAR,BXM,BYM,BZM,EYO
      COMMON ISEED,DY,DX,NIED,NIED1,NSUMO
C
      DO 4 J=2,NY1
         DO 5 I=1,NX
            EY(I,J)=-(PHI(I,J+1)-PHI(I,J-1))/(2.0*DY)
 5       CONTINUE
 4    CONTINUE
C
      DO 7 J=1,NY
      DO 6 I=2,NX1
            EX(I,J)=-(PHI(I+1,J)-PHI(I-1,J))/(2.0*DX)
 6    CONTINUE
 7     CONTINUE
C
      DO 8 J=1,NY
         EX(1,J)=-(PHI(2,J)-PHI(1,J))/DX
         EX(NX,J)=-(PHI(NX,J)-PHI(NX1,J))/DX
 8    CONTINUE
C
      DO 9 I=1,NX
         EY(I,1)=-(PHI(I,2)-PHI(I,1))/DY
c        EY(I,NY)=EY(I,1)
         EY(I,NY)=-(PHI(I,NY)-PHI(I,NY1))/DY
 9    CONTINUE
C
      RETURN
      END


C     ***********************************************************
C           SUBROUTINE MOVEI
C     ***********************************************************
      INTEGER SIGT,SIGR
      REAL ION
      COMMON/PAR/ELE(163840,5),ION(163840,5)
      COMMON/ARRAY1/PHI(129,65)
      COMMON/EFIELD/EX(129,65),EY(129,65)
      COMMON/ARRAY/RHO(129,65),RHOE(129,65),RHOI(129,65)
      COMMON/DEL/DVXI,VXIW(301),FIW(301),GIW(301),VDRI,DVXE,VDRE
     >          ,VXIO(301),FIO(301),GIO(301)
     >          ,VXEO(241),FEO(241),GEO(241)
      COMMON/VEX/XX(129),YY(65)
      COMMON TIME,NIJ
      COMMON NX,NY,NX1,NY1,PI,MAIN
      COMMON RATO,RATW,DELT,VELVAR,BXM,BYM,BZM,EYO
      COMMON ISEED,DY,DX,NIED,NIED1,NSUMO
C
      DO 1 L=1,NIED
         IF(ION(L,1) .GT. XX(NX)) GO TO 1
         IF(ION(L,1) .LT. XX(1)) GO TO 1
            NII=INT(ION(L,2)/DY)+1
```

```
               NJ=INT((ION(L,1))/DX)+1
                 SIGR=+1.
                 SIGT=+1.
                     DELA=ABS(ION(L,1)-XX(NJ))
                     DELB=ABS(ION(L,2)-YY(NII))
                     A1=DELA*DELB
                     A2=DX*DELB-A1
                     A3=DY*DELA-A1
                     A4=DX*DY-(A1+A2+A3)
                     TOTA=DX*DY
              EXPF=(A1*EX(NJ+SIGR,NII+SIGT)+A2*EX(NJ,NII+SIGT)+
     >   A3*EX(NJ+SIGR,NII)+A4*EX(NJ,NII))/TOTA
              EYPF=(A1*EY(NJ+SIGR,NII+SIGT)+A2*EY(NJ,NII+SIGT)+
     >   A3*EY(NJ+SIGR,NII)+A4*EY(NJ,NII))/TOTA
C
      IF( L .LE. NSUMO) THEN
      ION(L,3)=ION(L,3)+(EXPF+ION(L,4)*BZM-ION(L,5)*BYM)*DELT*RATO
      ION(L,4)=ION(L,4)+(EYO+EYPF-ION(L,3)*BZM+ION(L,5)*BXM)*DELT*RATO
      ELSE
      ION(L,3)=ION(L,3)+(EXPF+ION(L,4)*BZM-ION(L,5)*BYM)*DELT*RATW
      ION(L,4)=ION(L,4)+(EYO+EYPF-ION(L,3)*BZM+ION(L,5)*BXM)*DELT*RATW
      ENDIF
C
      XAX = ION(L,1)
      YAY = ION(L,2)
C
      ION(L,1)=ION(L,1)+ION(L,3)*DELT
      ION(L,2)=ION(L,2)+ION(L,4)*DELT
      IF( L .LE. NSUMO)THEN
      ION(L,5)=ION(L,5) + (ION(L,1)-XAX)*BYM*RATO
     >            - (ION(L,2)-YAY)*BXM*RATO
      ELSE
      ION(L,5)=ION(L,5) + (ION(L,1)-XAX)*BYM*RATW
     >            - (ION(L,2)-YAY)*BXM*RATW
      ENDIF
1     CONTINUE
C
      DO 111 L=1,NIED
        IF( ION(L,1) .GT. XX(NX) )THEN
           ION(L,1) = ION(L,1) - XX(NX)
        ELSE
           IF( ION(L,1) .LT. 0.0 )THEN
              ION(L,1) = XX(NX) + ION(L,1)
           ENDIF
        ENDIF
111     CONTINUE
C
      DO 112 L=1,NIED
        IF( ION(L,2) .GT. YY(NY) )THEN
           ION(L,2) = ION(L,2) - YY(NY)
        ELSE
           IF( ION(L,2) .LT. 0.0 )THEN
              ION(L,2) = YY(NY) + ION(L,2)
           ENDIF
        ENDIF
112     CONTINUE
C
      RETURN
      END
C     ***********************************************************
        SUBROUTINE MOVEE
C     ***********************************************************
      INTEGER SIGT,SIGR
      REAL ION
      COMMON/PAR/ELE(163840,5),ION(163840,5)
      COMMON/ARRAY1/PHI(129,65)
```

```fortran
      COMMON/EFIELD/EX(129,65),EY(129,65)
      COMMON/ARRAY/RHO(129,65),RHOE(129,65),RHOI(129,65)
      COMMON/DEL/DVXI,VXIW(301),FIW(301),GIW(301),VDRI,DVXE,VDRE
     >           ,VXIO(301),FIO(301),GIO(301)
     >           ,VXEO(241),FEO(241),GEO(241)
      COMMON/VEX/XX(129),YY(65)
      COMMON TIME,NIJ
      COMMON NX,NY,NX1,NY1,PI,MAIN
      COMMON RATO,RATW,DELT,VELVAR,BXM,BYM,BZM,EYO
      COMMON ISEED,DY,DX,NIED,NIED1,NSUMO
C
      DO 1 L=1,NIED
          IF(ELE(L,1) .GT. XX(NX)) GO TO 1
          IF(ELE(L,1) .LT. XX(1)) GO TO 1
              NII=INT(ELE(L,2)/DY)+1
              NJ=INT((ELE(L,1))/DX)+1
                  SIGR=+1.
                  SIGT=+1.
                      DELA=ABS(ELE(L,1)-XX(NJ))
                      DELB=ABS(ELE(L,2)-YY(NII))
                      A1=DELA*DELB
                      A2=DX*DELB-A1
                      A3=DY*DELA-A1
                      A4=DX*DY-(A1+A2+A3)
                      TOTA=DX*DY
              EXPF=(A1*EX(NJ+SIGR,NII+SIGT)+A2*EX(NJ,NII+SIGT)+
     >    A3*EX(NJ+SIGR,NII)+A4*EX(NJ,NII))/TOTA
              EYPF=(A1*EY(NJ+SIGR,NII+SIGT)+A2*EY(NJ,NII+SIGT)+
     >    A3*EY(NJ+SIGR,NII)+A4*EY(NJ,NII))/TOTA
C
          ELE(L,3)=ELE(L,3)-(EXPF+ELE(L,4)*BZM-ELE(L,5)*BYM)*DELT
          ELE(L,4)=ELE(L,4)-(EYO+EYPF-ELE(L,3)*BZM+ELE(L,5)*BXM)*DELT
C
          XAX = ELE(L,1)
          YAY = ELE(L,2)
          ELE(L,1)=ELE(L,1)+ELE(L,3)*DELT
          ELE(L,2)=ELE(L,2)+ELE(L,4)*DELT
          ELE(L,5)=ELE(L,5)-((ELE(L,1)-XAX)*BYM-(ELE(L,2)-YAY)*BXM)
1     CONTINUE
C
      DO 111 L=1,NIED
        IF( ELE(L,1) .GT. XX(NX) )THEN
           ELE(L,1) = ELE(L,1) - XX(NX)
        ELSE
           IF( ELE(L,1) .LT. 0.0 )THEN
              ELE(L,1) = XX(NX) + ELE(L,1)
           ENDIF
        ENDIF
111     CONTINUE
C
      DO 112 L=1,NIED
        IF( ELE(L,2) .GT. YY(NY) )THEN
           ELE(L,2) = ELE(L,2) - YY(NY)
        ELSE
           IF( ELE(L,2) .LT. 0.0 )THEN
              ELE(L,2) = YY(NY) + ELE(L,2)
           ENDIF
        ENDIF
112     CONTINUE
C
      RETURN
      END
C
CCCCCCCCCCCCCCCCCCCCCCCCCCCCCCCCCCCCCCCCCCCCCCCCCCCCCCCCCCCCCCCCCCCCCC
      SUBROUTINE EXCHANGE
CCCCCCCCCCCCCCCCCCCCCCCCCCCCCCCCCCCCCCCCCCCCCCCCCCCCCCCCCCCCCCCCCCCCCC
```

```
          REAL IONPX,IONPY
          REAL ION
          COMMON/PAR/ELE(163840,5),ION(163840,5)
          COMMON/ARRAY1/PHI(129,65)
          COMMON/EFIELD/EX(129,65),EY(129,65)
          COMMON/ARRAY/RHO(129,65),RHOE(129,65),RHOI(129,65)
          COMMON/DEL/DVXI,VXIW(301),FIW(301),GIW(301),VDRI,DVXE,VDRE
     >              ,VXIO(301),FIO(301),GIO(301)
     >              ,VXEO(241),FEO(241),GEO(241)
          COMMON/VEX/XX(129),YY(65)
          COMMON TIME,NIJ
          COMMON NX,NY,NX1,NY1,PI,MAIN
          COMMON RATO,RATW,DELT,VELVAR,BXM,BYM,BZM,EYO
          COMMON ISEED,DY,DX,NIED,NIED1,NSUMO
C
          TPI = 2.*PI
          DO 100 I = 1,2
          NSUMO1 = NSUMO - 1

          IONEX = INT(RAN(ISEED) * NSUMO1) + 1
          IONPX = ION(IONEX,1)
          IONPY = ION(IONEX,2)

          DO 10 J=IONEX,NIED1
            DO 10 K = 1,5
              ION(J,K) = ION(J+1,K)
10        CONTINUE

          ION(NIED,1) = IONPX
          ION(NIED,2) = IONPY

          RND = RAN(ISEED)
          DO 50 K=1,241
           DIFF1 = FIW(K) - RND
           IF(DIFF1 .GE. 0.0) GO TO 55
50        CONTINUE
55        ION(NIED,3) = VXIW(K)
          VPAR = 0.0589*SQRT(-LOG(1-RAN(ISEED)))
          TPAR = TPI*RAN(ISEED)
          ION(NIED,4) = VPAR*SIN(TPAR)
          ION(NIED,5) = VPAR*COS(TPAR)

          NSUMO = NSUMO - 1

100       CONTINUE
          RETURN
          END

C
CCCCCCCCCCCCCCCCCCCCCCCCCCCCCCCCCCCCCCCCCCCCCCCCCCCCCCCCCCCCCCCCCCCC
          SUBROUTINE FOURN(DATA,NN,NDIM,ISIGN)
CCCCCCCCCCCCCCCCCCCCCCCCCCCCCCCCCCCCCCCCCCCCCCCCCCCCCCCCCCCCCCCCCCCC
          REAL*8 WR,WI,WPR,WPI,WTEMP,THETA
          DIMENSION NN(NDIM),DATA(16384)
          NTOT=1
          DO 11 IDIM=1,NDIM
            NTOT=NTOT*NN(IDIM)
11        CONTINUE
          NPREV=1
          DO 18 IDIM=1,NDIM
            N=NN(IDIM)
            NREM=NTOT/(N*NPREV)
            IP1=2*NPREV
            IP2=IP1*N
            IP3=IP2*NREM
            I2REV=1
```

```fortran
          DO 14 I2=1,IP2,IP1
             IF(I2.LT.I2REV)THEN
                DO 13 I1=I2,I2+IP1-2,2
                   DO 12 I3=I1,IP3,IP2
                      I3REV=I2REV+I3-I2
                      TEMPR=DATA(I3)
                      TEMPI=DATA(I3+1)
                      DATA(I3)=DATA(I3REV)
                      DATA(I3+1)=DATA(I3REV+1)
                      DATA(I3REV)=TEMPR
                      DATA(I3REV+1)=TEMPI
12                 CONTINUE
13              CONTINUE
             ENDIF
             IBIT=IP2/2
1            IF ((IBIT.GE.IP1).AND.(I2REV.GT.IBIT)) THEN
                I2REV=I2REV-IBIT
                IBIT=IBIT/2
             GO TO 1
             ENDIF
             I2REV=I2REV+IBIT
14        CONTINUE
          IFP1=IP1
2         IF(IFP1.LT.IP2)THEN
             IFP2=2*IFP1
             THETA=ISIGN*6.2831853/(IFP2/IP1)
             WPR=-2.*SIN(0.5*THETA)**2
             WPI=SIN(THETA)
             WR=1.
             WI=0.
             DO 17 I3=1,IFP1,IP1
                DO 16 I1=I3,I3+IP1-2,2
                   DO 15 I2=I1,IP3,IFP2
                      K1=I2
                      K2=K1+IFP1
                      TEMPR=(WR)*DATA(K2)-(WI)*DATA(K2+1)
                      TEMPI=(WR)*DATA(K2+1)+(WI)*DATA(K2)
                      DATA(K2)=DATA(K1)-TEMPR
                      DATA(K2+1)=DATA(K1+1)-TEMPI
                      DATA(K1)=DATA(K1)+TEMPR
                      DATA(K1+1)=DATA(K1+1)+TEMPI
15                 CONTINUE
16              CONTINUE
                WTEMP=WR
                WR=WR*WPR-WI*WPI+WR
                WI=WI*WPR+WTEMP*WPI+WI
17           CONTINUE
             IFP1=IFP2
          GO TO 2
          ENDIF
          NPREV=N*NPREV
18     CONTINUE
       RETURN
       END
```